SELF-ASSEMBLY, THERMOTROPIC AND LYOTROPIC BEHAVIOUR OF SYNTHETIC BRANCHED-CHAIN ALKYLMALTOSIDES

NUR ASMAK NABILA BINTI SAARI

FACULTY OF SCIENCE
UNIVERSITY OF MALAYA
KUALA LUMPUR

2018

SELF-ASSEMBLY, THERMOTROPIC AND LYOTROPIC BEHAVIOUR OF SYNTHETIC BRANCHED-CHAIN ALKYLMALTOSIDES

NUR ASMAK NABILA BINTI SAARI

DISSERTATION SUBMITTED IN FULFILMENT OF THE REQUIREMENTS FOR THE DEGREE OF MASTER OF SCIENCE

DEPARTMENT OF CHEMISTRY
FACULTY OF SCIENCE
UNIVERSITY OF MALAYA
KUALA LUMPUR

2018

UNIVERSITY OF MALAYA

ORIGINAL LITERARY WORK DECLARATION

Name of Candidate: Nur Asmak Nabila Binti Saari

Matric No: SGR150018

Name of Degree: Master of Science

Title of ~~Project Paper/Research Report~~/Dissertation/~~Thesis~~ ("this Work"):

SELF-ASSEMBLY, THERMOTROPIC AND LYOTROPIC BEHAVIOUR OF SYNTHETIC BRANCHED-CHAIN ALKYLMALTOSIDES.

Field of Study: Physical Chemistry

I do solemnly and sincerely declare that:

(1) I am the sole author/writer of this Work;
(2) This Work is original;
(3) Any use of any work in which copyright exists was done by way of fair dealing and for permitted purposes and any excerpt or extract from, or reference to or reproduction of any copyright work has been disclosed expressly and sufficiently and the title of the Work and its authorship have been acknowledged in this Work;
(4) I do not have any actual knowledge nor do I ought reasonably to know that the making of this work constitutes an infringement of any copyright work;
(5) I hereby assign all and every rights in the copyright to this Work to the University of Malaya ("UM"), who henceforth shall be owner of the copyright in this Work and that any reproduction or use in any form or by any means whatsoever is prohibited without the written consent of UM having been first had and obtained;
(6) I am fully aware that if in the course of making this Work I have infringed any copyright whether intentionally or otherwise, I may be subject to legal action or any other action as may be determined by UM.

Candidate's Signature Date:

Subscribed and solemnly declared before,

Witness's Signature Date:

Name:

Designation:

SELF-ASSEMBLY, THERMOTROPIC AND LYOTROPIC BEHAVIOUR OF SYNTHETIC BRANCHED-CHAIN ALKYLMALTOSIDES

ABSTRACT

Maltose sugar (normally used widely in candy industry and intravenous injection) in this study is used as the hydrophilic headgroup attached to the Guerbet chain. The effect of chain branching on glycolipid thermotropic and lyotropic phases was investigated for a series of synthetic β-D-maltosides derived from Guerbet alcohols, whose total hydrocarbon chain length ranged from C_8 to C_{24}. Synthesis and characterisation of various branched-chain glycolipids have been attempted as these are suitable models for further study on the structure and mechanism of cell membrane. Since natural glycolipids compound have limited availability and require extensive syntheses, similar compounds that can mimic the property of natural materials were synthesised for applications in the field of biophysics and biotechnology. The branched-chain glycolipids have been reported to produce the inverse liquid crystal structures inducing various changes in the physicochemical properties of the disaccharide-based glycolipids self-assembly. The compounds were synthesised to a high purity and their liquid crystalline phases were characterised using differential scanning calorimetry (DSC), optical polarising microscopy (OPM), and small-angle X-ray scattering (SAXS). Thermal investigations of all anhydrous Guerbet maltosides showed that they do not form solid crystals but undergo a glass transition upon temperature change in the range of 35 to 53 °C. The glassy crystalline structure turns into the liquid crystalline structure upon heating or addition of water. In thermotropic studies, the lamellar phase formation is prominent in shorter chain length analogues while the longer chain compounds exhibit more frustrated form of self-assembly in the formation of metastable state, polymorphism and inverse bicontinuous cubic structure (*Ia*3*d*) as the synthesised maltosides possess two opposing features from the headgroup (energetic) and the chain branching (entropic) which are

equally dominant, resulting in the self-assembly to become frustrated and compromised to give a particular thermotropic polymorphism. The clearing temperatures of these branched-chain maltosides are in the range of 138 to 233 °C. The high clearing temperatures are due to the extensive hydrogen bond network in the head group region. Lyotropic studies show that the phase formation is dominated by lamellar phase for the longer chain compounds. Normal micellar solution was also observed in the shortest chain length maltosides due to the enlargement in hydrated maltose headgroups as observed from the SAXS investigations.

Keywords: Liquid crystals, Guerbet glycolipids, polymorphism

SIFAT SWA PENYUSUNAN, TERMOTROPIK DAN LIOTROPIK DALAM ALKILMALTOSIDA RANTAI BERCABANG SINTETIK

ABSTRAK

Dalam kajian ini, maltosa (kebiasaannya diguna secara meluas dalam industri makanan dan suntikan intravena) telah digunakan sebagai kepala hidrofilik yang dicantumkan pada rantaian Guerbet. Kesan rantai bercabang terhadap fasa termotropik dan liotropik glikolipid telah dikaji bagi siri β-D-maltosida sintetik yang dihasilkan daripada alkohol Guerbet, dengan kepanjangan rantai hidrokarbon dalam lingkungan C_8 hingga C_{24}. Sintesis dan pencirian pelbagai glikolipid rantai bercabang telah dilakukan kerana sebatian ini sesuai dijadikan model bagi kajian struktur dan mekanisme membran sel. Oleh kerana sebatian glikolipid semulajadi adalah terhad malah sintesisnya juga mencabar, sebatian yang menyerupai glikolipid semulajadi telah disintesis bagi aplikasi dalam bidang biofizik dan bioteknologi. Glikolipid rantai bercabang dilaporkan mampu membentuk struktur cecair hablur songsang yang mendorong pelbagai perubahan dalam sifat fizikokimia glikolipid yang berasaskan disakarida. Sebatian ini disintesis pada ketulenan yang tinggi dan fasa cecair hablur disiasat dengan menggunakan kalorimetri imbasan perbezaan (DSC), mikroskopi pengutuban optik (OPM) dan serakan sinar-X bersudut-kecil (SAXS). Penyiasatan termal terhadap semua maltosida Guerbet anhydrous menunjukkan bahawa mereka tidak membentuk kristal tetapi menjalani peralihan kaca dalam lingkungan 35 hingga 53 °C apabila berlaku perubahan suhu. Struktur kristal berkaca berubah menjadi struktur kristal cair pada pemanasan atau penambahan air. Dalam keadaan kering, pembentukan fasa lamela jelas kelihatan dalam analog rantai yang lebih pendek manakala sebatian berantai panjang mempamerkan bentuk yang lebih tertekan dalam swa penyusunan dengan pembentukan keadaan metastabil, polimorfisma dan struktur kubus dwiselanjar songsang (*Ia*3*d*) kerana maltosida yang disintesis mempunyai dua ciri yang bertentangan hasil daripada kumpulan kepala (energetik) dan

rantai bercabang (entropik) yang sama dominan, dan menyebabkan swa penyusunan menjadi sukar dan akhirnya berkompromi untuk memberikan polimorfisma termotropik. Suhu pembersihan maltosida rantai bercabang ini adalah dalam lingkungan 138 hingga 233 °C. Suhu cair yang tinggi adalah disebabkan oleh rangkaian ikatan hidrogen yang kuat di rantau kumpulan kepala. Penambahan air menunjukkan pembentukan fasa yang didominasi oleh fasa lamela dan juga cecair misela dalam sebatian rantai paling pendek disebabkan pembesaran dalam kumpulan kepala maltosida yang terhidrat seperti mana yang diperhati daripada SAXS.

Kata kunci: Cecair hablur, glikolipid Guerbet, polimorfisma

ACKNOWLEDGEMENTS

Alhamdulillah, first and foremost to His Most Gracious and Merciful for bestowing me with many opportunities in this life and health to carry on. Many thanks to my parents for their steadfast love and unyielding support to me.

To my supervisors, Dr Noor Idayu Mat Zahid and Prof Rauzah Hashim whose passions and knowledge are literally my beacon in the midst of confusion and uncertainty in this long voyage. Thank you for your patience, guidance and life message that you taught me in this journey. I will strive to make use of the knowledge and lessons that I learnt from you in my next endeavour.

Joining the Fundamental and Frontier Sciences in Nanostructure Self-Assembly has been a source of inspiration for me as it introduced me to a group of scientists and their collaborators who work extensively over the years contributing to their respective field. Although I cannot name every one of them, I would like to thank them as a group for inspiring me with their commitment.

To my friends and comrades that walk along this path with me; Melonney, Wan Farah Nasuha, Siti Syaidatul Atiqah and Azwa Amanina, thank you for all the shared laughs and the fruitful discussions. I wish all of us the best in our next venture.

I dedicate this thesis to all the pursuers of knowledge with the message of perseverance; and to the liquid crystals community, this work will not be complete without all of you. I share this accomplishment with my boisterous siblings which humour and aggravation are equally entertaining and the staple of my daily life.

TABLE OF CONTENT

LIST OF FIGURES

LIST OF TABLES

LIST OF EQUATIONS

LIST OF SYMBOLS AND ABBREVIATIONS

2D	:	Two-dimension
α	:	Alpha
β	:	Beta
Col	:	Hexagonal columnar phase
CPP	:	Critical Packing Parameter
Cr	:	Crystalline phase
D	:	Discotic phase
DSC	:	Differential Scanning Calorimetry
ΔH	:	Enthalpy
G	:	Glassy phase
H_I	:	Normal hexagonal phase
H_2	:	Inverse hexagonal phase
Iso	:	Isotropic phase
L_c	:	Lamellar crystal phase
L_1	:	Normal micellar solution
L_α	:	Lamellar liquid crystal phase
$L_{\alpha G}$	:	Lamellar glass
Mal	:	Maltose
M_α	:	Centered rectangular phase
$\hat{n}$	:	Director axis
N	:	Nematic phase
N*	:	Nematic cholesteric
NMR	:	Nuclear Magnetic Resonance
OPM	:	Optical Polarising Microscope

p	:	Packing parameter
q	:	Scattering vector
S	:	Order parameter
SmA	:	Smectic A phase
SmC	:	Smectic C phase
SAXS	:	Small-Angle X-ray Scattering
T_c	:	Clearing temperature
T_g	:	Glass transition temperature
TLC	:	Thin Layer Chromatography
T_m	:	Melting temperature
V_2	:	Inverse bicontinuous cubic phase
WAXS	:	Wide-Angle X-Ray Scattering

LIST OF APPENDICES

CHAPTER 1 : INTRODUCTION

1.1 General Introduction

Glycolipids are amphiphilic molecules with unique properties that arise from the coexistence of hydrophilic sugar head group and hydrophobic alkyl chain, often results in the formation of highly self-organised structures. They are usually found on the exterior of the lipid layer of cell wall, where they are involved in intercellular recognition processes, signal transduction, transmembrane transportation, cell adhesion and other specialised functions. Some of them are capable of self-assemble when dry (thermotropic) as well as when solvated (lyotropic) and their role in membrane processes are better understood through their lyotropic and surfactant properties. Their structural role can be best recognised through a systematic examination of these molecules varying in head group geometry and their hydrocarbon chain structures (Goodby, 1998; Kitamoto et al., 2009; Manickam Achari et al., 2012).

Various works have probed into the study of sugar-based glycolipids compound that include the study of glycolipids with monosaccharide and disaccharides head groups. In this study, the focus is one the disaccharide glycolipids in order to further understand the effect of larger and more polar head group on the liquid crystalline properties. Using the branched-chain Guerbet glycolipids, the effect of chain-branching on the self-assembly structure can also be investigated. From this study, significant differences in the liquid crystalline behaviours and self-assemblies were expected from the disaccharides glycolipids as compared to its monosaccharide counterparts.

In this work, a series of disaccharide compounds were synthesised using an established method for the synthesis of branched-chain glycolipids (Hashim et al., 2006). Their thermotropic and lyotropic behaviour will be determined using Optical Polarising

Microscopy (OPM) by temperature variation and water penetration respectively. The OPM measurement is a qualitative study and the results will be supported and complemented by Differential Scanning Calorimetry (DSC) and Small Angle X-Ray Scattering (SAXS) (Kitamoto et al., 2009). The phases are designated using the standard lyotropic nomenclature in both dry and fully hydrated states because the molecules involved are amphiphilic rather than mesogenic (Brooks et al., 2011; Hamley, 2000).

1.2 Liquid Crystals as Special Phase of Matter

1.2.1 Definition

Liquid crystals exhibit dual properties of both liquid and solid. In solid state, molecules usually possess both positional and orientational orders. Hence molecules are compelled to occupy a specific space in a lattice and to direct their molecular axes in specific directions. Molecules in a simple liquid crystal behave in a similar manner to those in the liquid phase, in which they do not possess positional order in three dimensions. This makes them flow like a liquid. However, in a liquid crystal phase they possess a certain degree of orientational order and also a certain degree of positional order, whereby, most of the crystal order is diminished and this is observed by comparing the latent heat value of crystal to liquid crystal phase transition and that of liquid crystal to liquid. The value of crystal to liquid crystal transition is typically 250 J/g while that of a liquid crystal to liquid transition typically is about 5 J/g. Nevertheless, the small amount of order in liquid crystal is reflected in their mechanical and electromagnetic properties which is usually found in crystals (Collings & Hird, 1997; Helfrich & Heppke, 1980).

The liquid crystalline phase is a state of matter with properties of liquid and a solid-crystal. The phases formed by liquid crystals are called mesophase. This phase describes the molecular organisation of the materials that exists in between the perfect

three-dimensional position and orientation ordering of solid, and also the lack of long-range orientational order usually found in isotropic liquids. In general, liquid crystal compounds are made of a rigid moiety and one or more flexible molecule residue. The rigid part will align the molecules into a specific direction while the flexible parts impart fluidity into the liquid crystalline system (Garidel et al., 2015).

As previously mentioned, the property of liquid crystals that distinguishes them from liquids is the presence of a small degree of order among the molecules. This order makes the phase anisotropic like a crystal. Solids on the other hand can either be isotropic or anisotropic, depending on the molecules occupying the lattice sites and the crystal lattice itself (Collings & Hird, 1997; Kocks et al., 1998). Amorphous solids like plastic crystals and glass are examples of isotropic solid where they have the same physical properties in all directions due to the absence of periodic pattern in three dimensions (Kelly & Knowles, 2012) and the phase is orientationally disordered (Suga, 2011).

1.2.2 Order in Liquid Crystal

One of the most basic properties in the simplest liquid crystal phase is that the molecular axis tends to point along a preferred direction. This preferred direction is called the director and denoted by the unit vector $\hat{n}$. Order parameter, *S*, describes to what degree the long axis of the molecule is aligned with the director on average (Collings & Hird, 1997; de Gennes & Prost, 1993). The values of *S* between 0 and 1 describe degrees of ordering between completely isotropic and completely ordered (Wojtowicz et al., 1975). In liquid crystal, the director is also called the average direction. Figure 1.1 illustrates the director and the angle of a mesogen to the preferred director. Order parameter, *S*, can be calculated with the following the equation:

$$\boldsymbol{S = \left\langle \frac{3\,cos^2 - 1}{2} \right\rangle}, \qquad \textbf{Equation 1.1}$$

where S is the order parameter and θ is the angle between a particular mesogen's long axis and the director (preferred direction) in liquid crystal phase is shown in Figure 1.1.

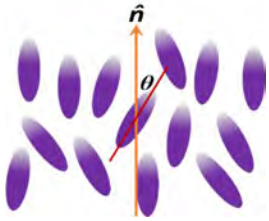

Figure 1.1: The director, $\hat{n}$ of liquid crystals mesogens and θ indicates the angle for order parameter, S.

1.2.3 Defects

A typical liquid crystal assembly usually contains many points where the director is undefined. Technically, these are defects in the structure and could be point, lines, or sheets where the direction of orientational order discontinuously changes. Point defects tend to occur in restricted geometries and at surfaces. Sheet defects usually occur when the change in orientational order is continuous over a slab containing the sheet (Collings & Hird, 1997; Singh & Dunmur, 2002). These defects give rise to the textures of the liquid crystalline phases when observed under the OPM as shown in Figure 1.2 and Figure 1.3. This is the basis of liquid crystal phase identification by OPM textures, since different liquid crystal structures will have different defects. In Figure 1.2, the point defects result in the Schlieren texture of nematic liquid crystals and in Figure 1.3, the hyperbole and ellipse disclination result in the focal conic texture of smectic liquid crystals.

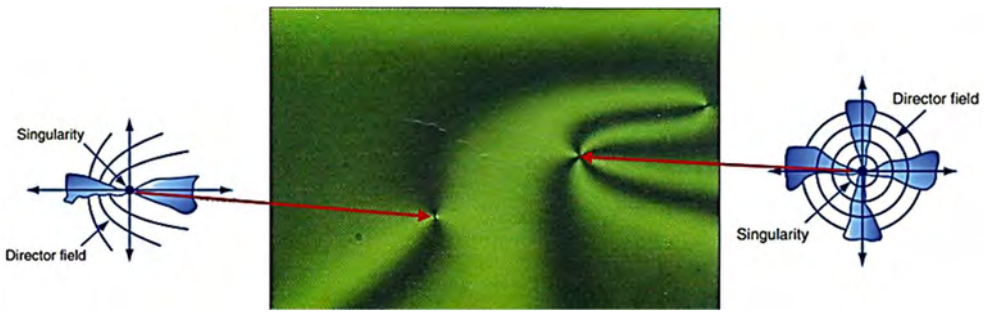

Figure 1.2: The 2-brush and 4-brush defects. OPM textures and figures were redrawn from (Dierking, 2003) and (Goodby, 2012) respectively.

Figure 1.3: Smectic layers growing from two points due to a disclination in the shape of an ellipse (Collings, 2002).

1.3 Structure-Property Relationship in Liquid Crystals

The molecular structure of a liquid crystal compound and various combinations of it structural units affect the observed mesophase and their physicochemical properties. The following rules must be taken into consideration in molecular design in order to obtain compounds with the desired liquid crystalline properties (Collings & Hird, 1997).

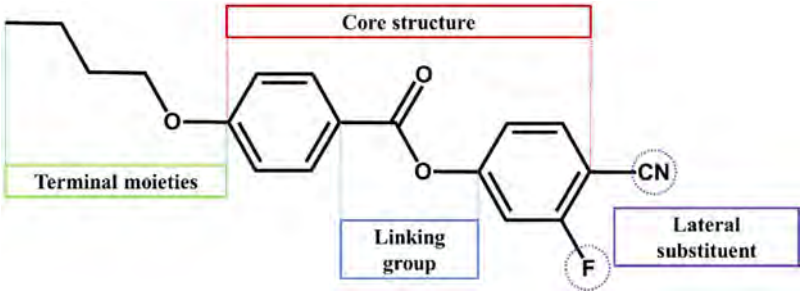

Figure 1.4: 4-Cyano-3-fluorophenyl 4-butoxybenzoate, an example of liquid crystal mesogen and its structural units.

Core Structure

The rigid part was constructed from ring units and often includes linking groups and other lateral substitution to the ring. This unit can be made of aromatic core such as benzene rings or naphthalene, as shown in Figure 1.4 and also can be built from the alicyclic ring, such as the cyclohexane. The types of core; for example, in the case of phenyl or alicyclic ring greatly affect the formation of liquid crystal phase, physical properties and the liquid crystal transition (Singh & Dunmur, 2002). In this work, the rigid part of the molecule is made up of the pyranose sugar molecules, specifically the maltoside.

Terminal Unit

Terminal groups other than hydrogen are always employed in liquid crystal systems. Commonly use end group units are small polar substituents like the cyano group and long, straight hydrocarbon chains (usually alkyl or alkoxy). The alkyl/alkoxy chain provides flexibility to the rigid core structure and stabilising molecular orientation for mesophase formation. Polar groups on the other hand give substantial intermolecular attraction force to stabilise molecular orientation. Variations in the transition temperatures are observed with different length of terminal chain. Longer alkyl chain enhances nematic phase stability and promotes smectic phase formation and their flexibility also disrupt the molecular packing required for mesophase generation. On the other hand, chain branching disrupts the molecular packing and reduces melting points and phase stability. Terminal moieties also greatly affect the physical properties of mesogens (Collings & Hird, 1997; Singh & Dunmur, 2002).

Linking Group

Linking groups are structural units that connect one part of a core to another and also used to link the terminal chains to the core. The use of bridging group induces flexibility in the material and a useful method in reducing the transition temperature and destabilising the mesophase (Singh & Dunmur, 2002). It is used to extend the length and polarisability of anisotropy, hence enhancing the stability of the liquid crystal phase and producing wider range of liquid crystalline phase. There are numerous examples of linking groups including the azo, imine, ester and etc (Collings & Hird, 1997).

Lateral Substituent

Lateral substituents are usually attached on the linear axis of the molecule, be it on the rigid core or on the terminal alkyl chain such as the alkyl group and other moieties such as fluoro and cyano. Lateral substitution provides subtle disturbance on the molecular

packing, henceforth reducing the liquid crystal phase stability. In many cases, this disruption is favourable for various applications, for example in ferroelectric host materials (Collings & Hird, 1997).

1.4 Brief Perspective on Liquid Crystal History

Due to the widespread use of smartphones and digital flat screens in modern living, liquid crystals are pervasive in our daily life in the form of LCD devices. In this technology, perhaps the most prevalent liquid crystals manifest from the monophilic type. On the contrary, the basic unit of the living organisms are made from the lyotropic amphiphilic liquid crystals which makes these materials far more important in life sciences and biotechnology. It is of great interest to look into the timeline of liquid crystals development to further understand the interest in the discovery of these materials.

The discovery is often attributed to an Austrian botanist Friedrich Reinitzer in 1888, who experimented with cholesterol-related-compound and learnt that the compound possesses two melting points (Reinitzer, 1989). He later sent the compound to Otto Lehmann, a physicist working in Germany studying the crystallisation properties of various substances for further inspection. Lehmann observed Reinitzer's samples with his microscope mounted with special temperature-controlled stage and noted the similarity with one of his own samples (Lehmann, 1889). He referred them as soft crystals and later, as crystalline fluid. Once he is convinced that the opaque phase possesses both liquids and solids properties, he started to call them liquid crystals. Lehmann's discovery sparked the interest on liquid crystals in France. In 1922, George Friedel introduced the classification scheme for liquid crystals; namely the nematic, smectic and cholesteric phases (Friedel, 1922). Friedel also coined in the terms used today to describe the liquid crystals including 'mesophase'. During the war years in 1930s and 1940s, the focus of liquid crystals experimentations was on their elastic properties, X-ray studies and the

effect of electronic and magnetic fields. After the Second World War (WWII), studies on liquid crystals slowed down due to the lack of discussion in textbook and the lack of its application at the time (Collings & Hird, 1997; Kumar, 2011).

Shortly after the WWII ended, research in liquid crystals bloomed across Europe. George W. Gray, one of the most prominent figures in liquid crystals field began the research on these materials in England around 1940s. His work led to better understanding in molecular designs in order to achieve compounds with higher thermal stability. In 1962, he wrote a book about liquid crystals (Gray, 1962) and successfully ignite the world's interest on this subject and subsequently received many awards and honours for his contributions in this field. Gray's book sparked the interest on the study of liquid crystals in United States in the 1960s. Glenn H. Brown of Kent State University initial research interest was on the structure of liquid crystalline phases as determined by X-ray crystallography. Later on, his research interest was more into the lyotropic and biological liquid crystals. One of Brown's greatest contribution was the establishment of the International Liquid Crystal Conference providing a platform for the scientists across the world to exchange ideas and information on this interesting subject matter (Castellano, 2005).

Research on liquid crystals exploded during 1970s and 1980s. Scientifically, liquid crystals are important phases for various phenomena in biological contexts. Its investigation involves multidisciplinary approach involving physicists, chemists, biologists and engineers working together to unearth the properties of these intriguing materials. Technologically, liquid crystal displays can be implied to have swept over the modern world and our daily life with the various creations, developments and innovations of the electronic devices (Kumar, 2011).

On the other hand, in the cosmetic industry, the surfactant market is expected to worth 39.86 billion USD by 2021 with the increasing awareness for environmental-friendly base

material that drives the market of bio-based surfactants (marketsandmarkets.com, October 2016). Amphoteric sugar-based surfactants are among the suitable candidates that fulfils the green features requirement.

In the topic of amphiphilic carbohydrate liquid crystal, the observation of double melting point of certain alkyl glucopyranoside by Fischer and Helferich in 1911 and also the observation of optical texture on the aqueous dispersions from the extract of tuberculosis bacteria by Koch marked the first contribution on thermotropic and lyotropic behaviour respectively (Bonicelli et al., 1998; Vill, et al., 2000).

George A. Jeffrey looked into the potential of carbohydrates as model compounds to further understand the biological connection between the liquid crystal phase formation and membrane transport. He agreed with Fischer's observation that the thermotropic liquid crystal formation can be thought of as a two-stage melting process as the principal cohesive forces of carbohydrates are hydrogen bonds that melt at high temperature and the hydrocarbon that will melt at lower temperature as their cohesive forces are van der Waals. The difference between these two forces give rise to thermo-mesophases (Jeffrey, 1986).

1.5 Liquid Crystals Classification

Liquid crystals are often divided into two main groups; namely thermotropic and lyotropic liquid crystal. Thermotropic liquid crystals exhibit phase transition upon temperature variation while lyotropic liquid crystals' phase transitions occur upon variation of temperature and concentration of the compounds in solvent (Tschierske, 2002). Amphitropic liquid crystal is the term used to express the ability of a compound to form both thermotropic and lyotropic mesophases (Barón, 2001; Vill & Hashim, 2002).

There are various kind of molecules that can form liquid crystal phase. These anisotropic molecules (mesogens) can either be monophilic that are induced by shape anisotropy or amphiphilic where different parts of the molecules have very different solubility properties as per this thesis focus. The most common type of molecules that form liquid crystal phase is the rod-shaped molecules. These compounds fall under the category of monophilic liquid crystals and are called the calamitic liquid crystals and may manifest different liquid crystal phases. Some portion of the molecules must be fairly rigid to maintain the elongated shape for interactions that favour alignment (Collings & Hird, 1997).

Under monophilic category, where the molecules are usually made up of two parts; rigid and flexible, the common shape or structure of these molecules are rod-like (calamitic), bent-shaped (bad rods, boomerang, banana-like), disc-like (discotic) and also the polymer liquid crystals. Discotic liquid crystals are compounds with molecules possessing a disc-like profile, where one of the molecular axes is much shorter than the other two and the molecules are stacked one on top of the other in columns which in turn constituted to a 2D hexagonal arrangement. Discotic mesogens may exhibit various mesophase for example; hexagonal columnar, rectangular columnar, columnar oblique and etc. Both calamitic and discotic liquid crystals are called thermotropic liquid crystals as their liquid crystal phases are stable for a certain temperature interval (Collings & Hird, 1997; Kumar, 2011).

There are also liquid crystals that are formed from polymer molecules. Similar to calamitic and discotic mesogens, some part of the molecules must be rigid in order for it to be liquid crystalline. There are two major types of polymer liquid crystals; the main chain liquid crystal polymers (MCLCP) and the side chain liquid crystal polymers (SCLCP) as shown in Table 1.1. In MCLCP, the rigid structure units are separated by the flexible hydrocarbon chains while the rigid sections are attached to a long flexible

polymer chain by short flexible hydrocarbon chains in SCLCP (Collings & Hird, 1997) A third class of liquid crystal polymer can also be generated by inserting the mesogenic units both within the main chain and the side chain; namely as combined liquid crystal polymers (CLCP). The overall flexibility of the polymer chain can be influenced with the introduction of flexible spacers (e.g. alkyl chain) between the functional groups and the rigid mesogenic units (Singh & Dunmur, 2002).

On the other hand, amphiphilic molecules possess both polar and non-polar moieties in the same molecule as shown in Figure 1.5. These molecules will aggregate to form various structures in normal or inverse phase depending on the molecular structure and the type of solvent (Collings & Hird, 1997).

Amphiphilic molecules form slightly different liquid crystalline phase than the calamitic and discotic liquid crystals. Micelles (Figure 1.6) or vesicles (Figure 1.7) may be formed at low concentration. There is orientational and/or positional order of the molecules within the structure, however there is no overall order for the micelles and vesicles themselves. Hence, these structures are not considered as liquid crystal. At higher concentration, micelles and vesicles may change to ordered structures such as lamellar, hexagonal and cubic (Collings & Hird, 1997).

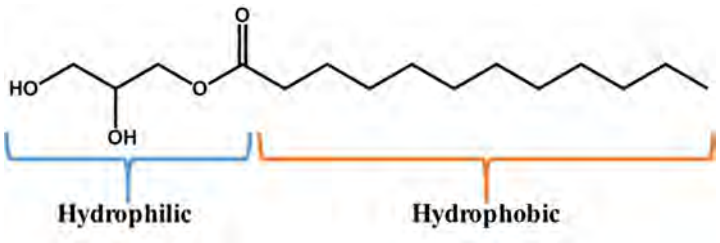

Figure 1.5: Schematic representation of a typical amphiphile; glycerol monolaurate.

Table 1.1: Mesogenic compounds and their phase behaviour with the illustrations of their respective self-assembly structures.

Liquid Crystal Mesogen	Self-assembly structure
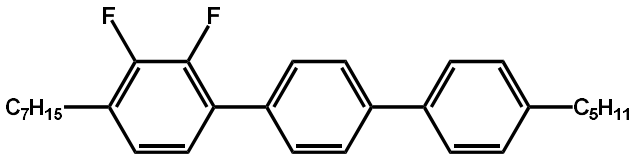 2,3-difluoro-4-heptyl-4"-pentyl-1,1':4',1"-terphenyl **Cr 56.0 SmC 105.5 SmA 131.0 N 136.0 Iso**	
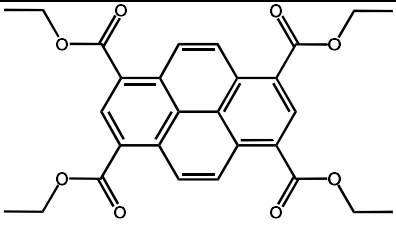 tetraethyl pyrene-1,3,6,8-tetracarboxylate **Cr 190 Col 204 Iso**	 Discotic
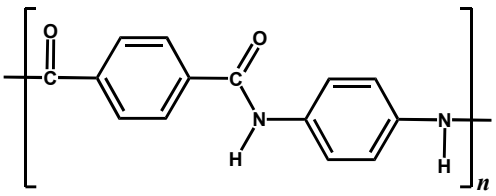 Kevlar	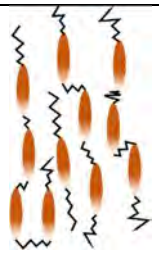 Main chain liquid crystal polymer
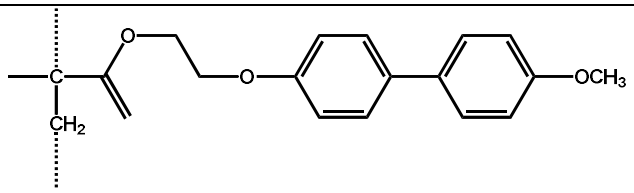 4-(2-((3,3-dimethylpent-1-en-2-yl)oxy)ethoxy)-4'-methoxy-1,1'-biphenyl **G 120 N 152 Iso**	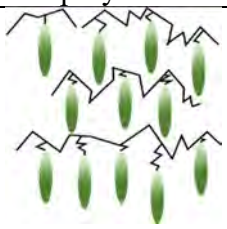 Side chain liquid crystal polymer
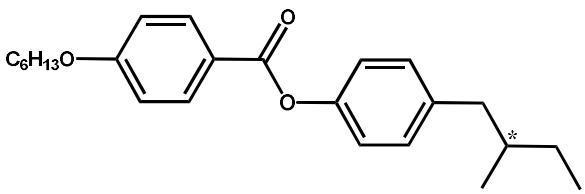 4-(2-methylbutyl)phenyl 4-(hexyloxy)benzoate **Cr 38 (SmA 17 N* 37) Iso**	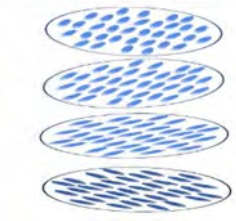 Chiral nematic

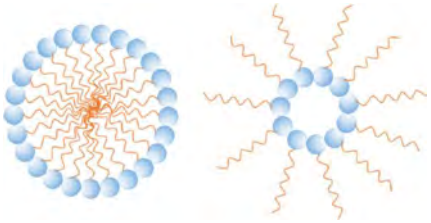

Figure 1.6: Cross-section of normal micelle (left) and inverse micelle (right).

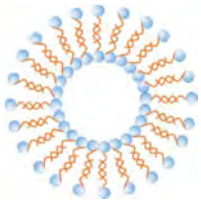

Figure 1.7: Cross-section of vesicle.

1.6 Liquid Crystal Phases

1.6.1 Monophilic

Monophilic mesogens typically exhibit thermotropic liquid crystalline properties. The nematic (N) phase as shown in Table 1.1 of the calamitic liquid crystal is the simplest liquid crystal phase where the molecules only maintain the orientational order with the absence of the positional order. In Smectic A (SmA) and Smectic C (SmC) phases as illustrated in Table 1.1, the molecules possess positional order since the molecules' centres of mass are arranged in layers with the latter are tilted. In the case of chiral molecules forming liquid crystal phase, a chiral phase liquid crystal will form. In chiral nematic phase, the director rotates in helical twist about an axis perpendicular to the director (Table 1.1). Apart from that, chirality induces the appearance of polar physical properties which is described by a vector or a third-rank tensor (Singh & Dunmur, 2002). This chiral phase is often called the cholesteric phase since many of the first compounds discovered with this phase were derivatives of cholesterol. Disc-like molecules form various liquid crystalline phases in the range of the simple nematic to the two-dimensional order of columnar. This type of molecules also forms chiral phase when chiral molecules are involved (Collings & Hird, 1997).

1.6.2 Amphiphilic

An amphiphile, as shown in Figure 1.5 refers to a molecule possessing a polar hydrophilic head group attached to a hydrophobic moiety. Amphiphiles essentially contain both hydrophilic and hydrophobic regions with different degree manifested by the hydrophilic and lipophilic balance (HLB). Amphiphilic molecules have great tendency to form liquid crystal when dissolve in solvent (usually water) (Brown & Wolken, 1979). In industry, amphiphiles are commonly used as detergent. The driving force to the various formation of these liquid crystalline phases is microphase separation as these compounds aggregate themselves into separate regions of lipophilic and hydrophilic moieties held together by van der Waals interaction and hydrogen bonding respectively (Garidel et al., 2015; Vill & Hashim, 2002; Vill et al., 2000).

Lyotropic liquid crystals is another category of liquid crystal where the liquid crystal phase appears upon mixing amphiphilic compounds with solvent. For these compounds, the concentration and the temperature of the mixed solutions are important to achieve a stable liquid crystal phase (Auvray et al., 2001). These amphiphiles will form ordered structures in both polar and non-polar solvents, forming the normal phase and inverse phase respectively (Collings & Hird, 1997). Contrary to thermotropic liquid crystals which appear upon temperature variation, lyotropic liquid crystal appear upon the addition of solvent as well as temperature.

1.6.3 Self-Assembly of Lyotropic Liquid Crystals

Similar to thermotropic liquid crystals, there are various phases of lyotropic liquid crystals. Generally, the lyotropic liquid crystal behaviours are extensively studied over the whole concentration range. The lamellar, hexagonal and cubic phases are among the most widely recognised lyotropic liquid crystals and their various structures has been classified by X-ray studies (Collings & Hird, 1997; Singh & Dunmur, 2002).

Lyotropic mesophase behaviour is very similar to the thermotropic behaviour with two additional parameters which are; solvent type and the concentration. Microscopy perhaps is a suitable technique to study the thermotropic behaviour. However, in lyotropic study, X-ray technique is usually employed due to the complication in determining the various mesophases such as a cubic phase which appears 'black' under the microscope.

Lamellar

The self-assembly system of a lamellar (L_α) lyotropic phase consists of bilayer made up of polar and non-polar counterparts correspondingly as shown in Figure 1.8. It is also known as 'neat phase'. The polar head groups are separated by a layer of water. Typically, lamellar mesophase only exist down to 50% surfactant. Below 50% surfactant, transition from lamellar phase to hexagonal or isotropic micellar solution may occur. In term of viscosity, lamellar phase is less viscous than hexagonal phase despite containing less water due to its parallel layers that capable of sliding with ease over each other during shear (Collings & Hird, 1997; Singh & Dunmur, 2002).

Hexagonal

As implied by its name, the hexagonal phase has a molecular aggregate that corresponds to the hexagonal arrangement as depicted in Figure 1.8. This phase has similar birefringent texture with its thermotropic counterpart when viewed under polarising microscope. The two types of hexagonal lyotropic liquid crystal phases are normal hexagonal phase (H_1) and inverse hexagonal phase (H_2). The hexagonal phase is made up of micellar cylinder of indefinite length packed in a hexagonal arrangement. The inverse hexagonal phase typically has a smaller diameter than the normal hexagonal phase as the non-polar chain may overlap resulting in closer-packed cylinders (Collings & Hird, 1997). Although hexagonal phase contains higher water content than lamellar phase, the phase is very viscous due to its molecular packing (Singh & Dunmur, 2002).

Cubic

Cubic phase formation is not as common as the lamellar or hexagonal phases. They occur in different regions in phase diagram and their exact structure may depend on their position in the phase diagram. They can be generated in the normal manner (water continuous) or from the inverse manner (non-polar chain continuous) and the aggregates are similar to micelles. The molecular aggregates can be spherical, cylindrical or ellipsoidal. The lack of shear plane within the structure that inhibits sliding movement results in the high viscosity of these phases. The molecular aggregates arrangement also results in optically isotropic structure when viewed under the polarising microscope imposing extra challenge in detection and identification of these phases (Collings & Hird, 1997).

Discontinuous cubic phases are formed when the polar microphases of each micelle are isolated as the results of domination in part of the molecules. In this phase, molecules with cone-shaped structure stick together to form spherical or slightly anisotropic micelles that arranged in a cubic face-centred lattice. An example of this cubic phase is *Fd*3*m* which can be found in xylose base glycolipids. The structural modification in xylose sugar which is a replacement of hydroxylmethyl unit in glucose head group with a proton leading to a smaller, weakly polar head group with a bulky hydrophobic tail. Consequently, the mean interfacial curvature becomes more negative and this promotes the formation of inverse spherical aggregates which is the main feature of *Fd*3*m* (Liew et al., 2015; Minamikawa & Hato, 1998). The xylose head group may also adopt stable pyranose and furanose conformations that are probably responsible in forming two non-equivalent inverse micelles which then self-assembled into the *Fd*3*m* cubic discontinuous phase (Bayach et al., 2016).

Another category of cubic phase classification is the bicontinuous cubic phase which contains two continuous networks of channels. These types of cubic phases are formed

when the plane of lamellar curve positively and negatively to give a zero-mean curvature structure which forms a continuous network of channels which are either polar or non-polar. A bicontinuous cubic phase is usually located in between the lamellar and the hexagonal phase (Vill & Hashim, 2002). The morphology of bicontinuous cubic phase can be described as infinite periodic minimal surfaces (IPMS) where the minimal surface is defined by the lipid bilayer centre. The IPMS observed in amphiphile-water system are namely; gyroid, diamond and primitive which correspond to space groups *Ia*3*d*, *Pn*3*m* and *Im*3*m* respectively (Kaasgaard & Drummond, 2006). The space group structures are illustrated in Figure 1.8.

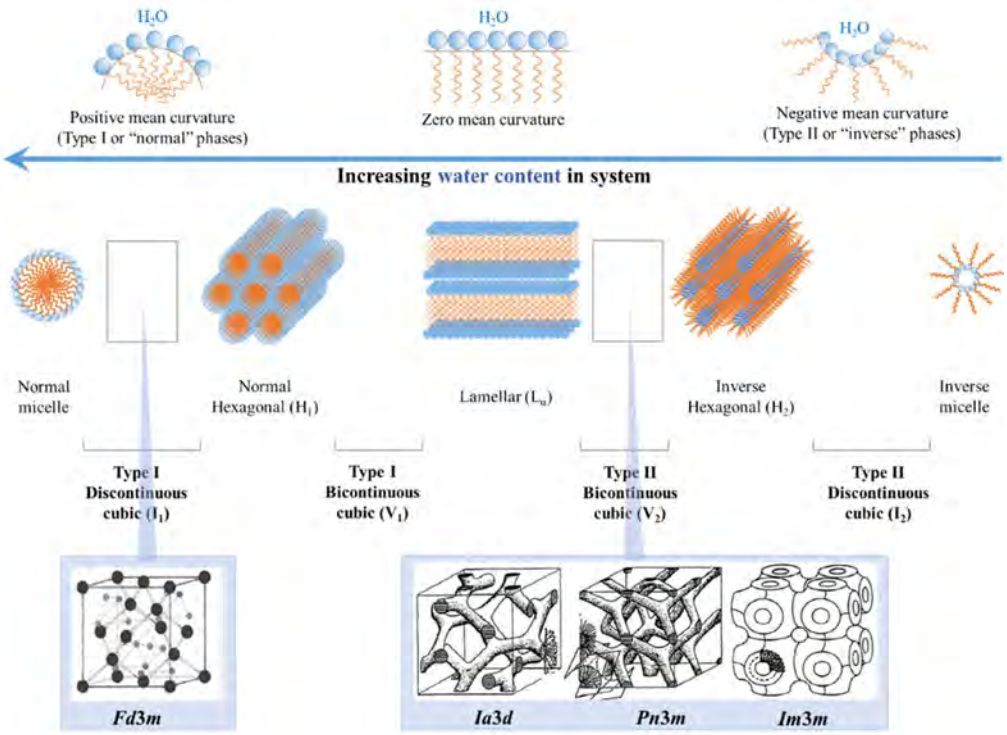

Figure 1.8: Schematic representation of lyotropic liquid crystal phases formed by amphiphiles in water in an ideal phase progression. Redrawn from (Kulkarni et al., 2011; Seddon, 1990; Wiesenauer & Gin, 2012).

1.7 Critical Packing Parameter (CPP), *p*

In aqueous dispersion, glycolipids tend to aggregate due to minimisation in the Gibbs free energy (Norde, 2011). The concentration at which the monomers start to form aggregate is called the critical micellar concentration (CMC). The type of aggregate

formed above the CMC is dependent on the relative sizes and geometries of the hydrophilic and hydrophobic moieties as proposed by Israelachvili (Israelachvili, 2015) who introduced the critical packing parameter (CPP), *p*, which is shown in Equation 1.2.

$$p = \frac{V}{al}\ , \qquad \textbf{Equation 1.2}$$

where *V* refers to the molecular volume of the hydrophobic region, *l* is the length of the fully extended hydrophobic part and *a* is the cross-sectional area of the hydrophilic moiety. If $p < {}^{1}/_{2}$, micellar and H_1 structure may be adopted. For *p* value between ${}^{1}/_{2}$ and 1, lamellar structure formation is favoured depending on the geometrical constraint, charge distribution, counter ions and hydration properties of the glycolipids. If $p > 1$, inverted structures are favoured for example, the H_2. In the critical range of $p = 1$, various phases may coexist resulting in phase transition upon slight changes to its physical properties (Nagarajan, 2002). Whilst CPP may predict the phase derived from a given molecular structure, various techniques such as OPM, X-ray and DSC are necessary to confirm the resulting mesophase.

1.8 Rules for Mesophase Formation in Amphiphilic Compounds

As mentioned previously, the driving force for liquid crystalline formation in amphiphiles is the microphase separation. The molecules need to possess the following factors to promote the microphase separation (Vill & Hashim, 2002):

(1) The molecules need at least two different molecular moieties that do not favour mixing with each other whether it be hydrophilic/hydrophobic or siloxane/hydrophilic and etc. The attraction difference between the two moieties is one of the contributing factors for the mesophase formation.

(2) The size of the molecular part is crucial where the ratio between volume and surface of the microphases must be large enough. Methanol does not form mesophase although possess an appearance similar to amphiphilic molecules as the polar and non-polar moiety are too small.

(3) The hydrophilic / hydrophobic balance should be fine-tuned to get the optimum liquid crystals behaviour and mesophases. Increasing the chain length will lower the clearing point due to the paraffin chain randomisation as a result of increased motion in hydrocarbon chain and vice versa.

(4) The allocation of the two different parts in the mesogens should provide fluidity to the mesophase system while separating the two different moieties.

(5) The mesogens need flexible parts for the formation of mesophase.

(6) Stereochemistry of the molecules may influence the properties.

1.9 Glycolipids as Amphiphilic Liquid Crystal

1.9.1 Glycolipids Definition

Glycolipids are lipids containing carbohydrate. Glycolipids are collectively part of a larger family of substances known as glycoconjugates, which are produced when carbohydrates interact with biomolecules such as lipids, proteins and etc. Glycolipids are produced when carbohydrates are covalently bonded to lipids. Glycolipids are amphiphilic molecules containing hydrophilic and hydrophobic parts that exist in nature but can also be synthesised chemically or enzymatically (Allen & Kisailus, 1992; Garidel et al., 2015; Zhang et al., 1996). Hence, the term glycolipid refers to any compound containing one or more monosaccharide residues bound by a glycosidic linkage to a hydrophobic moiety (Chester, 1999). An example of a natural glycolipid; glycosphingolipid was illustrated in Figure 1.11(b).

Various studies on simple monoalkylated glycolipids found that both size and detailed sugar structures such as the epimers and anomers control the thermotropic behaviour of glycolipids liquid crystals. An increased in the number of hydroxyl groups will increase the melting temperature, T_m, which is the transition temperature from hydrated solid to liquid crystal. It also increased the clearing temperature, T_c which refers to the transition temperature from liquid crystal into isotropic leading to a wider temperature range of the liquid crystalline phase (Manickam Achari et al., 2012; Vill & Hashim, 2002).

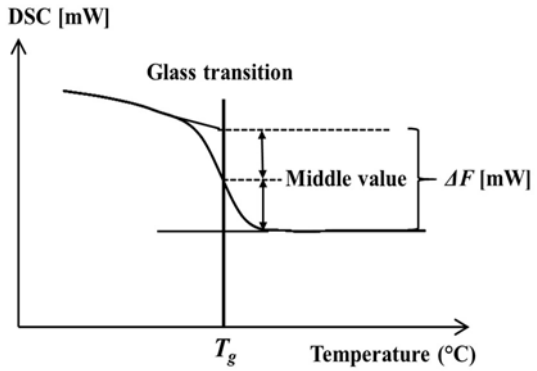

Figure 1.9: DSC thermogram of glass transition, T_g where the glass transition temperature, T_g is the middle value of the heat flow change, ΔF. Redrawn from (Ogawa & Osanai, 2012).

A glass is an amorphous solid which represents another class of solid-state phase which give rise to a glass transition, T_g (Kocherbitov & Söderman, 2004). Glass transition is defined as the point which the viscosity reaches a value in the range of 10^{11} to 10^{13} poise for non-polymeric liquids under supercooling without crystallisation and it is manifested directly by the rapid decrease of heat capacity C_p from liquid-like to crystal-like (Angell, 1995) as shown in Figure 1.9. Unlike normal sugar that readily form a glassy state below the glass transition temperature, T_g where the phase become frozen and both the molecular translational and rotational motions are drastically restricted (Kauzmann, 1948), glycoside sugars form glassy state with persisting long range order e.g. lamellar (Hashim et al., 2018; Kocherbitov & Söderman, 2004). This ordered glassy state may be called as 'glassy crystals' and 'glassy liquid crystals' (Kocherbitov &

Söderman, 2004). Such glasses possessing long range ordering and some other type of low molecular compounds have been reported to be used as unique host materials for optical and optoelectronic applications (Chen et al., 1999).

In biological science, the physical properties of the aggregates play an important role in living organisms as various biological processes for example the endo and exocytotic effect are dependent on the phase states and the transition temperatures (Garidel et al., 2015).

1.9.2 Glycolipids Liquid Crystal Mesophase

Glycolipids can form complex supramolecular structures in their pure form and in solvent due to their amphiphilic nature. The biocompatibility of glycolipids with nature encourage the various studies on these compounds for further understanding on natural processes such as membrane fusion and cell surface recognition processes (Curatolo, 1987; Ellens et al., 1986; Vill & Hashim, 2002; Vill et al., 2000). The most common phase in glycolipids is Smectic A (lamellar) for dry state. The formation of this phase requires comparable expanses (sizes) of sugars and paraffin. Monoalkylated carbohydrates usually exhibit this phase in thermotropic. Sugars with two alkyl-chain on the other hand will favour the thermotropic columnar (hexagonal) phase as the two-alkyl chain takes up more area than the sugar head. The two-alkyl chain creates a curvature of separation plane which is bent to a cylinder. The cylinders are filled with sugars and surrounded by the alkyl chains and packed into a hexagonal lattice (Vill & Hashim, 2002).

Amphiphilic molecules rarely formed ordered phases (SmB, SmG, Col_{ho}, etc.) and tilted phases (SmC, SmF, etc.) as the result of microphase separation in comparison to the monophilic liquid crystals. Interaction in monophilic liquid crystals is only in the means of the weak van der Waals forces, while in carbohydrates the interactions are in the form of dipoles and hydrogen bondings. The former results in small energy difference

between the tilted phases and non-tilted phases. Thus, monophilic liquid crystals are more sensitive to structural changes and exhibit various phase diversity than the amphiphilic liquid crystals (Vill & Hashim, 2002).

Comparing glycolipids birefringence with the Michel-Levy colour chart reveal that the studied glycolipids possess birefringence smaller than 0.05. The values are particularly small for molecules with long tails, suggesting more disorder in the hydrophobic chains than of the polar head. Previous studies found that the amphiphilic sugar lipids differ from the conventional thermotropic liquid crystals in various aspects (Liao et al., 2006).

From here onwards, this thesis shall adopt the standard lyotropic nomenclature (Hashim et al., 2018) in both dry and fully hydrated states because the molecules involved are amphiphilic rather than mesogenic (Brooks et al., 2011; Hamley, 2000).

1.9.3 Bonding in Glycolipids

Hydrogen bonding plays a central part in carbohydrate liquid crystals where the bond occurs between the head groups only. In amphiphilic mesogens, the hydrogen bonds form a network of fluctuating interaction and not fixed in certain position and time. On the other hand, hydrogen bonds in monophilic liquid crystals are static and directed. This result in the possibility of monophilic mesogens to exhibit nematic phases as oppose to the amphiphilic counterpart (Fukumasa et al., 1993). However, previous lyotropic study had described the possibility of amphiphilic carbohydrates to form the nematic and cholesteric phases (Vill & Hashim, 2002). The majorities of hydrogen bonding in glycolipids involved the intralayer and interlayer hydrogen bonding as shown in Figure 1.10 instead of intermolecular hydrogen bonding due to the orientational constraint of the thermotropic bilayer and the steric hindrance of the covalent structure of the lipid (Hashim et al., 2018).

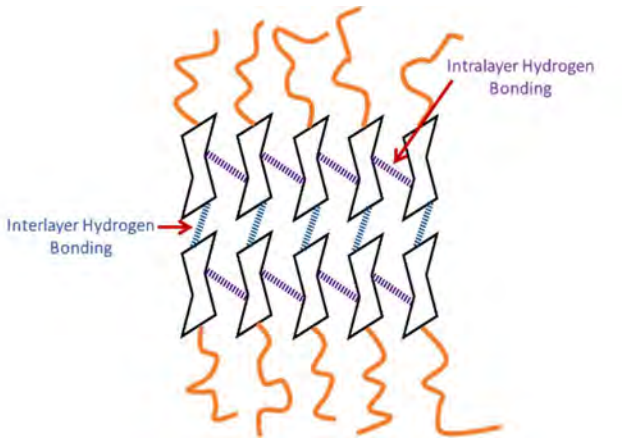

Figure 1.10: Hydrogen bonding in glycolipids. Redrawn from (Hashim et al., 2018).

1.9.4 Guerbet Glycolipids

Glycolipids from branched alkyl oligosaccharides comprising of primary alcohol branched in the 2-position and an oligosaccharide, covalently bond to the alcohol either α- or β-linkage may exhibit phase behaviours not found in the corresponding straight chain counterparts. An example of chemical structure for this type of glycolipids is shown in Figure 1.11(a). Depending on the choice of sugar head group and alkyl chain, different phases and properties may be exhibit by these compounds that could be useful for various applications requirements. These Guerbet compounds have structures which bio-mimic the natural lipids such as the glyco-glycerol lipids and ceramides (Hashim et al., 2018) and therefore are feasible to be applied for membrane studies (Ahmad et al., 2012).

Amphiphilic sugar lipids have lower birefringence and tend to align homeotropically on rubbed polymer surfaces as oppose to the conventional liquid crystals that tend to promote planar alignment. This property is due to the amphiphilic nature of the glycolipids where the polar head groups align themselves with the orientation that prevent contact with the hydrophobic surface. Branched-chain glycolipids give rise to a wide variety of mesophases with the tendency to form curve phases such as a columnar phase. They may also give both lamellar phase at lower temperatures and curve phases at higher temperature (polymorphism). The random orientation and greater flexibility of the tail

groups at higher temperature in amphiphilic molecules result in larger space occupation of the tail region compared to the polar heads which brings about stabilisation of the hexagonal phase (Liao et al., 2006). Many of the compounds are found to be in liquid crystal phase at room temperature (Hashim et al., 2006). However, recent literatures found that these compounds may actually exist in glassy phase at the room temperature (Hashim et al., 2018; Kocherbitov & Söderman, 2004; Ogawa et al., 2013).

Introduction of branched-chain in the compounds promotes inverse phase formation in their liquid crystalline states (Manickam Achari et al., 2012). Natural glycolipids usually comprised of two different alkyl chain that are attached through a linker to the sugar head group. Guerbet alcohols are racemic mixtures leading to the production of glycosides with diastereomeric mixtures. The key feature in the synthesis is the glycosidation where many branched-chain glycolipids form crystalline derivatives or co-crystallise as anomeric mixtures (Hassan, 2001). Hence, the purification process of these materials is tedious and usually involve chromatography. The impurities in the products are usually associated with anomeric contaminations as other contaminants are easily removed.

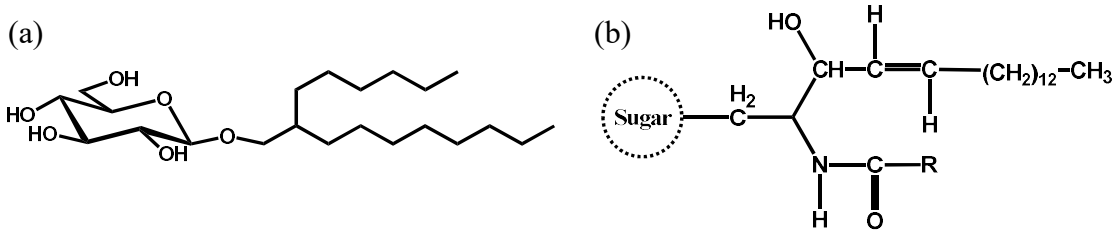

Figure 1.11: Structural comparison of (a) Guerbet glycolipid, the 2-hexyl-*n*-decyl-*β*-D-glycopyranoside with (b) natural glycolipid, glycosphingolipid (Hashim et al., 2018).

Chain branching brings about a few effects including liquid crystalline phase variation. Monoalkylated glycosides only exhibit L_α above the room temperature while Guerbet glycosides exist in a variety of ordered phases including the L_c, L_α, H_2 and V_2 even from below ambient temperature. They may also exhibit thermotropic polymorphism (Hashim

et al., 2006). Chain branching results in higher entropy that promotes hydrocarbon chain to 'melt' at lower temperature. This observation is similar to the presence of double bond in natural lipids. In addition, longer chain length Guerbet glycolipids tend to promote thermotropic non-lamellar and inverse curve phases (V_2 and H_2).

In general, chain branching is important to promote the stability of non-lamellar phases. The packing frustration resulting from the tendency of the hydrophilic region to form lamellar structure and the hydrophobic region to curve induces the formation of cubic phase. The asymmetric feature of the branched-chain in Guerbet glycolipids may be the necessary condition to stabilise the gyroid V_2 phase in excess water (Manickam Achari et al., 2012).

1.9.5 Monosaccharide Sugar Glycolipids

Advancement in synthetic procedures has enabled the synthesis of various glycolipids that mimic the nature ones as its natural counterparts are usually challenging to obtained and limited. An interest in the technological applications by amphiphiles with unique physical and chemical properties has rapidly accelerated various research in this area. Recent studies suggest that various aspects are accountable for the liquid crystalline phases formed (Mannock & McElhaney, 2004). Various monosaccharide sugar glycolipids of glucose and its various epimers (galactose, xylose, mannose) and their liquid crystalline properties has previously investigated showing numerous liquid crystalline phases of different types (Hashim et al., 2006; Liew et al., 2015; Patrick et al., 2018). Monosaccharide glucoside and its epimers glycolipids are shown in Figure 1.12.

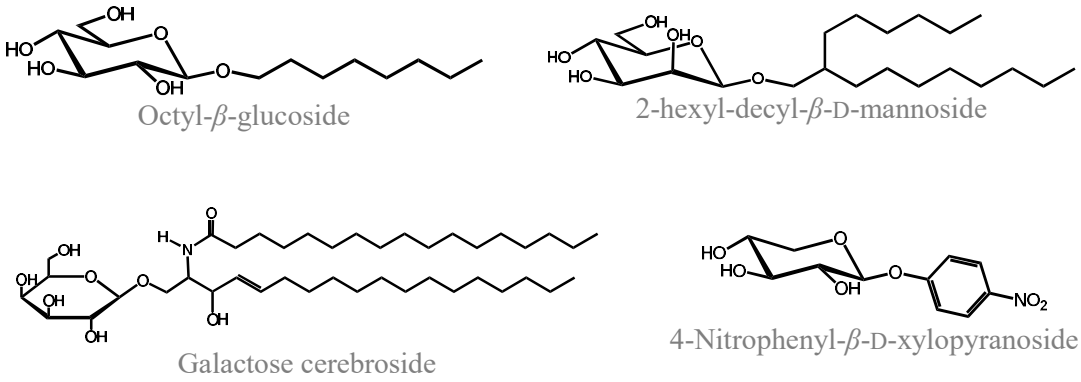

Figure 1.12: Examples of monosaccharide sugar glycolipids.

1.9.6 Disaccharide Sugar Glycolipids

Disaccharides are the simplest oligosaccharides with a number of them belong to the least expensive carbohydrates available and easily obtained by the means of polysaccharides hydrolysis. Maltose, as an example can be obtained in large quantities from starch (Lindhorst, 2000).

Maltose is applied in huge amount in the candy industry and incapable of crystallisation unless possessing purity more than 90% unlike the glucose that can crystallise even with high amount of impurities. It has also been used in intravenous injection to administer sugar for patients. It has also been utilised as a component in frozen desserts, sweetening agents, baking and brewing industry (Dziedzic & Kearsley, 1984). Introduction of substituents to the maltose sugar induce various changes in the physicochemical properties of the disaccharide compound.

Shorter chain Guerbet maltosides have a wider range of L_α compared to the corresponding glucosides due to the stronger electrostatic interaction via hydrogen bonding in the hydrophilic region. As the consequence, the transformation into another non-lamellar phase occurs at much higher temperature and requires more heat (Manickam Achari et al., 2012).

Typically, the longer branched chain of Guerbet glycolipids will self-assemble into the H_2 phase due to the dominating factor of chain volume and steric repulsion in the hydrophilic region. However, when the two opposing factors from the headgroup and the chain branching are equally dominant, the self-assembly becomes frustrated and compromised to give a thermotropic polymorphism. Polymorphism exhibits a series of phases from the L_α to non-lamellar phases upon heating (Manickam Achari et al., 2012). Examples of disaccharide sugar glycolipids are shown in Figure 1.13.

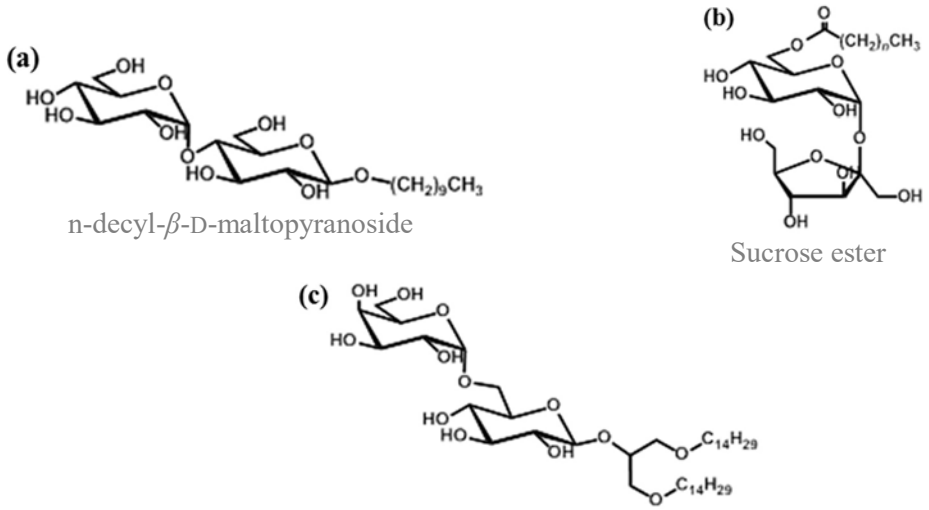

n-decyl-*β*-D-maltopyranoside

Sucrose ester

1,3-Di-*O*-tetradecyl-2-*O*-[6′-*O*-*α*-D-galactopyranosyl)-*β*-D-glucopyranosyl]-sn-glycerol

Figure 1.13: Examples of disaccharide sugars glycolipids from (a) maltose sugar; (b) sucrose; and (c) melibiose sugar.

1.10 Literature Review

Various works has included the studies on maltosides previously. Auvray et al. studied the thermotropic and lyotropic properties of five different surfactants. Perhaps one of the earliest and most comprehensive studies on the thermotropic and lyotropic studies of sugar glycolipids as potential surfactants has been conducted by Auvray et al. They studied the effects of anomericity, cylic or acyclic hydrophilic heads and the type of linkages between the hydrophilic and hydrophobic moieties. One of the studied compounds *β*-1-N-dodecyl-D-maltosides exhibit various liquid crystalline phases in the range of L_α, centered rectangular phase (M_α), gyroid lattice cubic phase (*Ia*3*d*) and

hexagonal from the lyotropic studies and phase diagram construction. These rich interpretations are contributed from the *β*-linkage in the compound (Auvray et al., 2001).

Garidel et al. on the other hand studied two compounds; maltoside and melibiose. They compared the effect of *α*(1→6) linkage in the former with the *α*(1→4) in the latter and their effect on physicochemical properties. They deduced that the bulky head group induces the formation of wedge-shaped conformation that facilitates the interdigitation of the hydrocarbon chain while increasing the van der Waals interactions (Garidel et al., 2008). Hashim et al. investigated the effect of chain branching on various types of monosaccharides and disaccharides glycosides. They found that the thermotropic structure of these compounds were similar to the lyotropic liquid crystalline behaviour that follow the critical packing parameter; proposing that the compounds can be considered as highly concentrated solutions (Hashim et al., 2006).

Ternary system of Guerbet glycosides has been studied by Nainggolan et al. that presented diverse phase progression for the glycolipid/*n*-octane/water system including the formation of rectangular ribbon phase in the monosaccharide head group (glucopyranoside) and only L_1 to L_α transition in the disaccharide head group (maltoside) (Nainggolan et al., 2009). On the other hand, Brooks et al. studied the effect of chain-branching on thermotropic and lyotropic behaviour of a series of synthetic Guerbet glucosides with total hydrocarbon chain in the range of C_8 to C_{24}. They found that in dry form the shorter chain compounds favour the formation of L_α while the longer chains tend to exhibit non-lamellar phases. These observations are due to the effect of chain branching that brings about a relatively large splay of hydrocarbon chains promoting the formation of non-lamellar phases (Brooks et al., 2011).

Zahid et al. reported the anomeric-epimeric related Guerbet glycolipids and their various liquid crystalline phases. Binary phase diagrams of the studied compounds were also constructed revealing various non-lamellar structures of the materials. The effect of

anomeric and epimeric of the sugar head group on the liquid crystalline behaviour of the compounds were studied and discussed (Zahid et al., 2013).

The novel properties of these Guerbet glycolipids may pose a great potential for technology application in the field of nano-emulsion and drug delivery. Ahmad et al. investigated the effect of Guerbet glycolipids inclusion for nano-emulsions stability utilising the formation of vesicles and hexosomes of the lyophilised glycolipids in water–surfactant dispersion (Ahmad et al., 2012). The study also included encapsulation of ketoprofen in a model drug delivery system. The favourable and fast release of the drug indicate the suitability of these compounds as co-additive for drug carriers (Ahmad et al., 2014).

1.11 Objectives of the Study

Fundamental understanding on the physicochemical and liquid crystalline properties of synthetic glycolipids liquid crystal requires systematic understanding with experimental characterisation which is the aim of this study. Henceforth, the following objectives are proposed in order to achieve the research main purpose:

(1) To synthesise a series of high purity (up to ~97%) Guerbet glycolipids of different alkyl chain length with maltose sugar as the designated head group.
(2) To investigate the thermal and mesomorphic behaviour of Guerbet maltosides using Differential Scanning Calorimetry (DSC) and Optical Polarising Microscopy (OPM).
(3) To determine the nanostructural parameters of the mesophases using the Small-Angle X-Ray Scattering (SAXS); hence construction of the binary phase diagram.

CHAPTER 2 : METHODOLOGY

2.1 Synthesis of Branched-Chain Glycolipids

The synthesis of various alkyl glycosides for this work followed a well-established procedure involving peracetylation, glycosidation and deacetylation previously reported (Vill et al., 1989; Vill et al., 2000) with some minor modifications (Hashim et al., 2006). This synthesis technique was chosen mainly for its anomeric selectivity, relatively inexpensive starting materials and straightforward experimental procedure.

In this study, the first peracetylation stage was not carried out as *β*-D-maltose octaacetate is commercially available in reasonable price. The glycosidation step involve the use of peracetylated sugars as the glycosyl donor. Boron trifluoride diethyl etherate is utilised as the Lewis acid catalyst in the glycosidation stage to catalyse the displacement of the acetoxy group at the C_1 position on the sugar molecules with the alkyl chain length of the Guerbet alcohol. The final step of deacetylation involved the removal of the acetate protecting group on the sugar head group using sodium methylate.

2.1.1 Materials

The peracetylated *β*-D-maltose octaacetate (98%) sugar was purchased from Carbosynth. The five Guerbet alcohols (97%) namely, 2-ethyl-1-hexanol, 2-butyl-1-octanol, 2-hexyl-1-decanol, 2-octyl-1-dodecanol and 2-decyl-1-tetradecanol used in the experiment were procured from Sigma-Aldrich. The catalyst boron trifluoride diethyl etherate, sodium methylate (97%) and ACS grade solvents which include dichloromethane, acetonitrile, *n*-hexane, ethyl acetate, ethanol and methanol were supplied from Merck. Ion exchange resin (Amberlite IR-120) and all the deuterated solvents used for the Nuclear Magnetic Resonance (NMR) study were also purchased from Merck. All chemicals and solvents were used without further purification.

Thin Layer Chromatography (TLC) technique is utilised (Boyd et al., 2000) for the detection of targeted components in a mixture of organic compounds. Hexane-ethyl acetate solvent system was used to develop the TLC. Merck silica gel 60 F_{254} coated on aluminium sheet was used together with charring solution of a mixture of ethanol, deionised water and sulphuric acid in the ratio of 90:8:2. The TLC plate was developed by immersing it in the solvent system followed by dipping the plate in the charring solution prepared in advance and finally the plate was burnt off using heat gun.

Flash column chromatography was utilised for purification of the synthesised products. The stationary phase is made up of the Merck Silica Gel 60 Å with the pore size of 0.035–0.070 mm. The mobile phase constitutes of hexane: ethyl acetate solvent system in a suitable ration as determined by the retention factor, R_f obtained from the TLC plate. The pressure inside the column is introduced manually to ensure a steady and continuous flow of the eluent with the help of the bellow pump.

In this study, NMR spectroscopy was used extensively for the determination of the anomeric purity and the chemical structure of the synthesised compounds. The proton attached at the anomeric C_1 gives a distinct doublet peak at different chemical shifts (approximately 0.4 ppm difference) according to whether their position is in the axial or equatorial orientation (Boyd et al., 2000). These observations verify that NMR spectroscopy is a very useful tool to discern the anomeric purity of the compounds. Both ^{1}H and ^{13}C-NMR spectra were recorded using Bruker Avance 400 NMR spectrometer and the measurements were conducted at 25 °C. The deuterated solvent used in the NMR measurement for the protected glycolipids are chloroform-d while for the deprotected glycolipids are methanol-d_4. The residual solvent peaks for chloroform-d recorded at 7.26 ppm for ^{1}H-NMR and 77.23 ppm for ^{13}C-NMR. For methanol-d_4, the residual peaks were recorded at 4.87 ppm and 49.15 ppm for ^{1}H-NMR and ^{13}C-NMR respectively.

2.1.2 General Glycosidation Procedure: Synthesis of *β*-Alkylmaltosides

β-D-maltose octaacetate (5 g, 7.4 mmol, 1 equiv.) was dissolved and stirred with the Guerbet alcohol (1.5–4.0 mL, 9.6 mmol, 1.3 equiv.) in 100 mL dichloromethane in the presence of catalyst boron trifluoride diethyl etherate (1.4 mL, 11.1 mmol, 1.5 equiv.) for four hours at room temperature. The reaction scheme is shown in Figure 2.1. The reaction progresses were monitored for every hour using TLC (hexane: ethyl acetate, 2:1) to determine the appearance of *β*-anomer glycolipids.

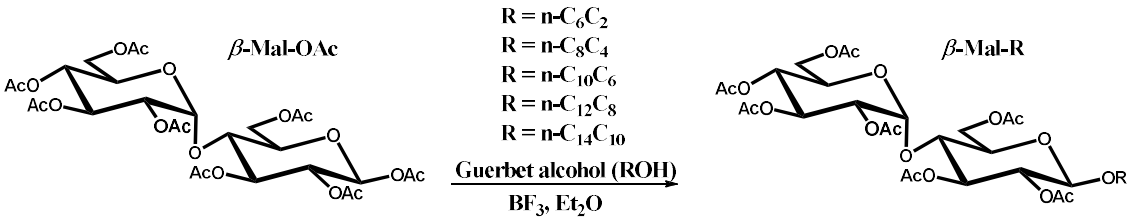

Figure 2.1: Synthetic scheme for glycosidation of maltoside.

After four hours, the reactions were stopped when *α*-anomer was detected on the TLC plate. The catalyst was neutralised by the addition of saturated hydrogen carbonate solution (twice) in separating funnel. The mixture was shaken thoroughly. This produced CO_2 as the by-product and the pressured gas was removed by opening and closing the stopcock repeatedly. The organic and aqueous layers were separated and the organic layer was collected and dried over anhydrous magnesium sulphate ($MgSO_4$). The anhydrous $MgSO_4$ was removed by gravity filtration and the filtrate was concentrated under reduced pressure. The product was further extracted with the solvent mixture of acetonitrile-hexane in the volume ration of 60:20 for two times to remove the remaining unreacted alcohols. The acetonitrile layer was collected and evaporated using rotary evaporator. The product obtained was further purified by flash column chromatography (hexane: ethyl acetate, 2.5:1). The eluent collected was monitored using the TLC plate with solvent system (hexane: ethyl acetate, 2:1). The solvent system was evaporated and

the chemical structures of the compounds collected were confirmed with ^{1}H-NMR and ^{13}C-NMR spectroscopy.

2.1.3 General Deacetylation Procedure

This step was carried out to remove the acetate protecting group on the sugar head group. The product from the glycosidation step was dissolved in methanol (1 g in 50 mL). Sodium methylate dissolved in methanol was added to the solution until the solution turned basic (pH 8–9). The reaction was left to stir at room temperature for overnight. The reaction scheme is depicted in Figure 2.2. The progress of the reaction can be monitored with TLC plate using the solvent system (hexane: ethyl acetate, 2:1). The solution was then neutralised with H^{+} ion exchange resins (Amberlite IR-120), filtered and evaporated. The compound was then dried in vacuum oven over phosphorus pentoxide at room temperature for at least 48 hours. The complete removal of the acetate protecting group can be confirmed with the absence of acetate peaks at approximately 2 ppm in ^{1}H-NMR spectra.

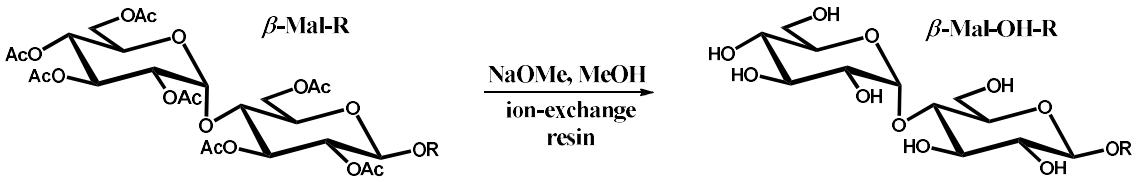

Figure 2.2: Synthetic scheme for deacetylation.

2.2 Characterisation of Liquid Crystal Behaviour

Liquid crystal materials give rise to various self-assembly structures with varying degrees of order. This complicates the determination of phase behaviours of the liquid crystalline structure as some of these compounds may exhibit polymorphism. As numerous thermal transitions may be present, a combination of techniques such as Differential Scanning Calorimetry (DSC), Optical Polarising Microscopy (OPM) and

Small-angle X-ray Scattering (SAXS) may be utilised for the precise interpretation of these behaviours (Ezquerra et al., 2009).

2.2.1 Differential Scanning Calorimetry (DSC)

DSC technique measures heat flow difference between the substance and reference as the function of temperature while the sample is subjected to a controlled temperature program. DSC applications include the determination of glass transition temperature, melting and crystallisation temperatures, purity determination, heat capacity measurement, characterisation of thermosets and measurement of liquid crystal transitions (Menczel & Prime, 2009).

A phase transition occurs when the thermodynamic of the system changes from one phase to another as a result of changing temperature and/or pressure and sometimes composition (Anthoy, 1987). In this technique, a software program is used to heat the furnace containing the sample and the reference holders at a linear heating rate. In the calorimeter, the sample is separated from direct contact with the sensor and encapsulated in a pan of a high thermal conductivity material. The difference between the two thermopiles (sensors) as shown in Figure 2.3 is proportional to the difference between the heat flow to the sample and reference. During measurement, the cell should be continuously purged with high-purity dry inert gas to ensure an inert and constant environment in the cell. In high temperature measurement, the gas functions as oxidation inhibitor and increases heat transfer to the sample. The DSC cell cross section is illustrated in Figure 2.4 (Menczel & Prime, 2009).

The thermal scheme for DSC experiment can be summarised as shown in Figure 2.5. As illustrated, one of the cell compartments contains the sample and the other cell contains the neutral reference. During the experiment, the temperature difference (or heat flux difference) is recorded as a function of time (Garden & Bourgeois, 2012).

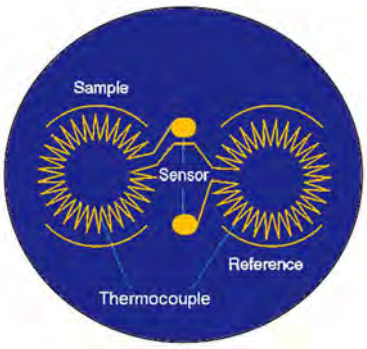

Figure 2.3: Schematic of thermopile used in Mettler Toledo calorimeter. Redrawn from (Menczel & Prime, 2009).

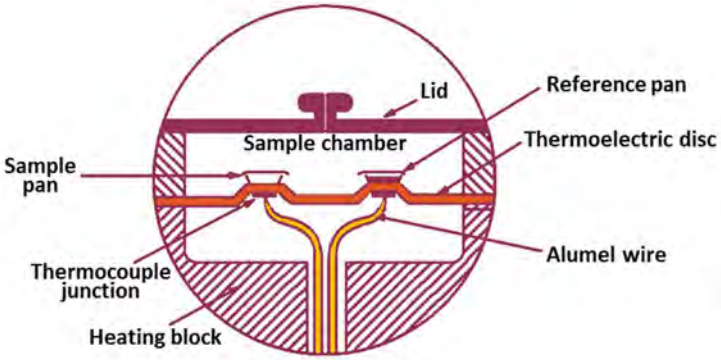

Figure 2.4: DSC cell cross section. Redrawn from (Menczel & Prime, 2009).

As the sample is heated, cooled or held isothermally, DSC analyser measures the energy changes and the temperature when these changes take place. The energy changes enabled the quantitative determination of the transition temperature that occurs in the sample. The sample preparation is relatively simple and considered as one of the advantages of this technique where the sample to be measured can be easily encapsulated with little or without preparation (Gabbott, 2008).

DSC measures the heat flow, which is the flow of energy into and out of the sample as a function of temperature or time and usually reported in the units of mW or mJ/s on the *y*-axis. The convention display for the heat flow curve is downwards direction for endotherm and upwards direction for exotherm. The values from the heat flow measurement enabled the identification of the range of transition that may occur in the sample as it is heated or cooled. The actual value of the heat flow may vary upon the

effect of the reference and is not absolute (Gabbott, 2008). In liquid crystal material study, DSC gives the information of the phase transition temperature and the associated enthalpy for first order phase transition. In this study, DSC complements the OPM since the former is unable to provide the information on the phase type of the liquid crystalline structures formed.

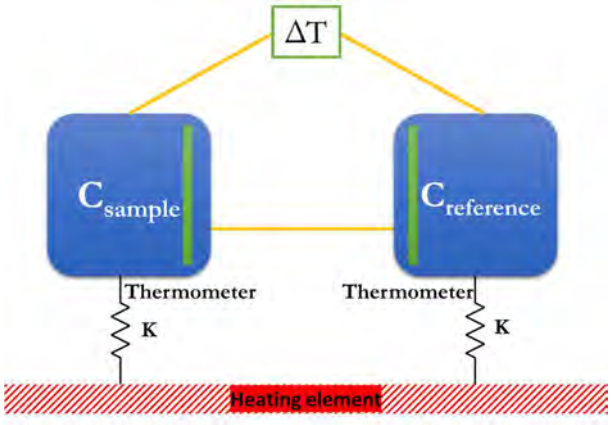

Figure 2.5: Thermal scheme of DSC experiment. Redrawn from (Garden & Bourgeois, 2012).

Measurement

For DSC measurement, 4–8 mg of dried sample was weighed accurately and encapsulated into the 40 µL aluminium crucible. The DSC analyser used was DSC 822^e, Mettler Toledo equipped with Haake EK90/MT intercooler. An inert environment was maintained during calibration and sample measurement by nitrogen purging to minimise potential oxidation. The instrument was calibrated with Indium standard for heat flow calibration, temperature calibration and furnace calibration. Indium was selected as the choice of standard due to its high precision of fusion value repetition (up to 0.1%) and can be reheated many times as long as it was not heated above 180 °C (Gabbott, 2008). The samples were subjected to repeated heating and cooling at the rate of 5 °C/min in a temperature range from of −50 °C up to 250 °C.

2.2.2 Optical Polarising Microscopy (OPM)

An optical polarising microscope allows the determination of both thermotropic and lyotropic behaviour of the compounds, by observing different textures in different phases of liquid crystals. Other functions of optical polarising microscope are also to identify and differentiate between isotropic and anisotropic media since it provides the information on both phase transition temperatures and phase type (Collings, 2002). Nature of the phase can be characterised by a particular observed texture. The manifestation of these unique textures is due to the presence of defects within the structure as the sample texture is viewed between crossed polarisers. Characteristic textures or structural defects observed in the anisotropic phase determine the phase type as shown in Figure 1.2 and Figure 1.3.

Polarisation refers to the limitation of the wave oscillation. A polariser only allows light oscillating in one direction to pass through it. Some compounds possess the property of double refraction (birefringence) where the incoming light is split into different optical axes where the latter will travel at different speed. When this light is recombined, such in the case OPM, interference will occur and with the aid of microscope a visual interferogram is formed at the back focal plane of the objective. The properties of this interference figure are the characteristics of the molecular properties of a material. The underlying physical principle is the alteration of light speed by interaction of light with different functional group in the molecule. Amorphous or glassy state refers to solid material lacking the long-range repeating pattern although they may possess the short-range order such as in the case of liquid crystals. Some compounds may exhibit polymorphism and this property is the ability of chemicals to arrange themselves into different geometric patterns that are physically stable in the solid state. In general, this technique is based on the fact that light travel at different speeds in different directions in the sample (Carlton, 2011).

Optical polarising microscope is designed to observe and photograph specimens that are visible due to their anisotropic character. The polarised light that passed through the birefringence sample will be broken out into two polarised rays; right angles to each other, travelling at different velocities and termed as ordinary and extraordinary rays. As these two rays are out of phase, they are later then recombined with constructive and destructive interference when they passed through the analyser as illustrated in Figure 2.6 (Robinson & Davidson, 2016; Wood, 1977).

A typical setup of optical polarising microscope is shown in Figure 2.6. It comprises of a halogen light source, that reflected upwards by the mirror to pass through the lens and the light is linearly polarised by the polariser that usually can be rotated by 360°. The light then enters condenser for optimal imaging of the sample. The condenser provides a uniform light illumination on the sample that achieved by aperture iris adjustment (Dierking, 2003).

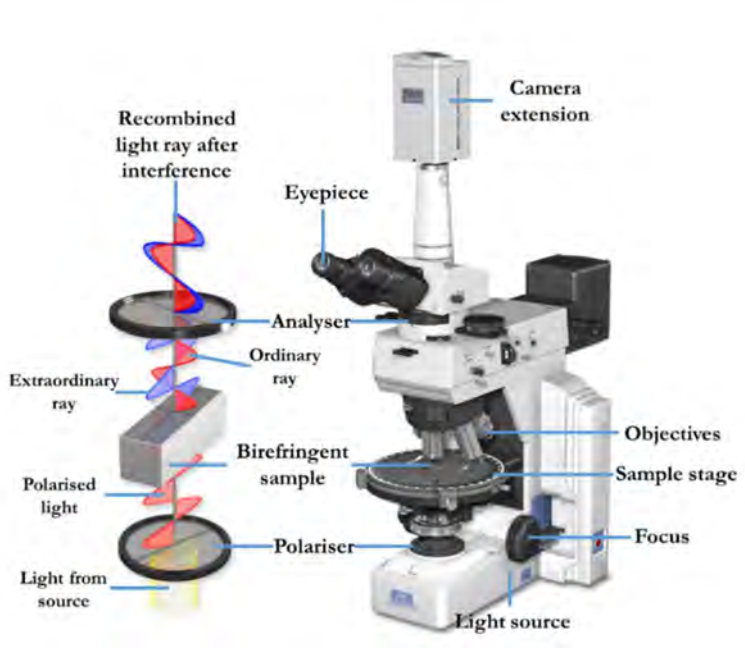

Figure 2.6: Setup of optical polarising microscope. Redrawn from (Robinson & Davidson, 2016).

For liquid crystal study, the microscopes are usually equipped with rotatable stage mounted with hot stage for temperature variation study. The coarse knob and fine knob

can be adjusted for optimum image viewing. The transmitted light that passes through the samples will enter the objectives with various magnification functions, usually X5 for low magnification, X10 and X20 for medium magnifications; and X50 for high magnification. After passing through the objective, the light will enter the analyser (second polariser) that is aligned 90° to the polariser (Dierking, 2003).

Thermotropic Study

The thermotropic behaviours of the samples were studied by drying the samples in the vacuum oven over phosphorus pentoxide for at least 48 hours to remove all the trace water as the sugar glycolipids are hygroscopic. Then, a small amount of the dried sample was then placed on the glass slide and covered with a thin glass cover slip and mounted onto the hot stage for temperature variation study. The sample was then heated to its isotropic temperature at the rate of 5 °C/min and then cooled down to room temperature at the rate of −2 °C/min. The first thermal cycle purpose is to produce a flat, coherent and even sample layer and to remove any remnant of crystallinity in the sample. The phase transition temperatures were recorded and the sample texture images were captured during the second heating (5 °C/min) and cooling (−2 °C/min) cycle.

Lyotropic Study

Lyotropic behaviour of the sample was carried out in an almost similar method to the thermotropic study of the compounds where the samples to be studied was placed in between the glass slide and cover slip and subjected to heating (5 °C/min) and cooling (−2 °C/min) to create a uniform sample surface. Deionised water droplet was then added to the edge of the cover slip and allowed to come in contact with the sample. The water will enter the sample via capillary force action creating a concentration gradient of excess water at the cover slip edge to neat surfactant under the glass cover slip.

Measurement

OPM study of the thermotropic and lyotropic liquid crystalline behaviour of the synthesised glycolipids were studied with Olympus BX51 polarising microscope equipped with Mettler Toledo FP82HT Hot Stage and temperature controller (FP90 Central Processor) linked to camera Olympus DP26. The images were captured under magnification factor of 10, 20 or 50 and viewed between two crossed polarisers. The cellSens standard software was used for image analysis and storage.

2.2.3 Small-Angle X-Ray Scattering (SAXS)

X-ray scattering technique can provide information on the structures and dynamics of large molecular assemblies in low-ordered domain (Ezquerra et al., 2009). The long-range order of the structure appears in the low-angle region of the scattering pattern in SAXS and crucial in determining the mesophase of the liquid crystal. The various liquid crystal mesophases possess long-range translational ordering with different symmetry that give rise to unique series of Bragg reflections which are characteristics of the phase symmetry (Tyler et al., 2015). SAXS is a powerful tool in determination of the thermotropic and lyotropic liquid crystalline structure. It is a probe-free and non-invasive technique with simple sample preparation and reasonable measurement time.

X-ray is produced when high-energy beam electrons penetrate through the valence band electrons and interact with the inner-shell electrons. If enough energy is transferred, the inner-shell electrons will be ejected; leaving a hole in the inner shell. The atom is said to be in ionised state (excited state). The ionised atom can return to the ground state by filling the inner shell hole with an electron from the outer shell. This transition results in emission of either X-ray or Auger electron. The emission energy is the difference of energy between the two electron shells involve and is unique to each particular atom

(Williams & Carter, 2009). The ionisation process is illustrated in Figure 2.7. The X-ray will interact with the sample and the interaction follows the Braggs' Law.

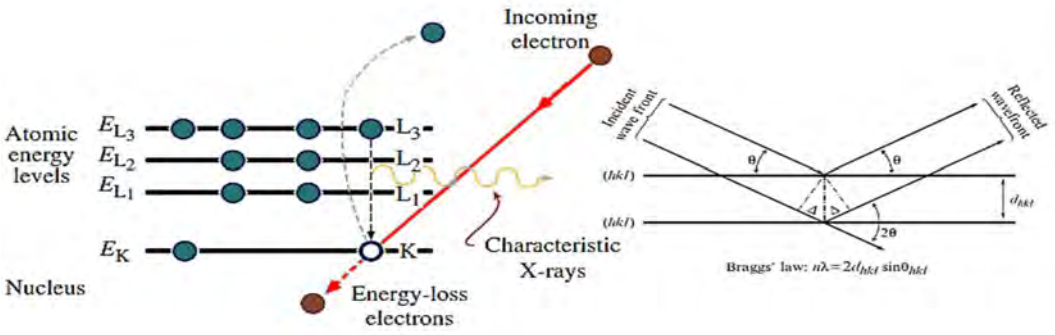

Figure 2.7: The ionisation process (Williams & Carter, 2009) and the geometric illustration of the Braggs' law (Pecharsky & Zavalij, 2009).

Amphiphilic molecules (compounds possessing both hydrophilic and hydrophobic properties) such as glycolipids can spontaneously self-assemble into various liquid crystalline structures with long-range and short-range interactions or disorders. Scattering patterns that appear in SAXS give information on the long-range orders of the structures and can be used to determine the phase symmetry and the lattice parameter of a particular liquid crystal assembly. At present, X-ray scattering is the only experimental technique that gives structural information down to Angstrom length scales (Tyler et al., 2015). X-ray scattering has been proven to be a useful technique in biological membrane research which includes membrane topological study, mechanical properties of lipid/water system and also lipophilic agents/drug interaction (Pabst et al., 2013). Small-angle scattering patterns are continuous in nature unlike the crystalline diffraction peaks. The key principle in this spectrometry is the fundamental Bragg's law as shown in Equation 2.1. From the Bragg's peak position, the system's gross morphology can be determined (Pabst et al., 2013). Braggs' law is visualised as shown in Figure 2.7 where the incident wavelength is diffracted by the discrete, parallel lattice plane in the crystal separated by distance, *d*.

$$n\lambda = 2d\,sin\theta = \frac{4\pi}{q}\,sin\theta, \qquad \textbf{Equation 2.1}$$

where n is the order of the reflection, λ is the wavelength of the X-ray radiation, d_{hkl} is the distance between the repeating planes in the lattice (d-spacing) and 2θ is the angle between the incident beam and the scattered beam. The X-ray scattering can also be expressed in term of scattering vector, q. Schematic diagram of the instrument inner component is illustrated in Figure 2.8 showing the scattering vector, incident beam and the scattered beam for further clarification on the inner working mechanism.

From Equation 2.1, angle of diffraction θ varies inversely with d of the diffracting lattice. It can also be noted that the scattering of nanometer and micrometer scale objects mainly appear in small-angle regime <5°. Hence, the name of this technique. In SAXS experiment, the fundamental of the instrument is to separate the intense, unscattered direct X-ray beam from the relatively weaker scattering from the sample at small angle 2θ.

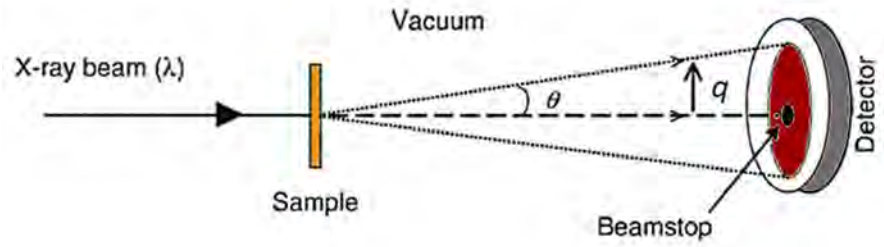

Figure 2.8: Schematic layout of SAXS setup depicting the incident and scatters rays, the angle of diffraction, θ and the scattering vector, q. Redrawn from (Borsali & Pecora, 2008).

A common experimental setup is illustrated in Figure 2.9. The setup is similar to the classic pinhole camera. From the X-ray source, the desired wavelength is selected and directed to pass through collimator before hitting the sample (Laver, 2012). Some of the radiation ray will be scattered by the sample and detected on the 2D detector. The 2D area detectors used in X-ray instrumentations are designed to have high detection efficiencies (>80%) and need to be shielded from the intense unscattered primary beam that may saturate and damage the detector. The beamstop is placed in front of the detector for these

reasons (Laver, 2012). Moreover, the entire Peltier system is put under vacuum to avoid absorption and scattering by air (Borsali & Pecora, 2008).

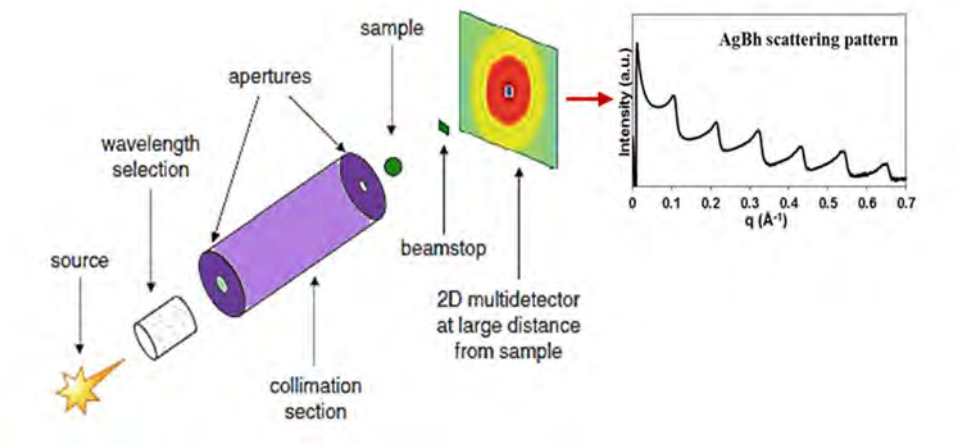

Figure 2.9: Schematic diagram of SAXS. The scattering pattern of silver behenate was shown as an example. Diagram redrawn from (Laver, 2012).

When the collimated X-ray beam hit the sample, the irradiated sample's electrons will scatter the X-ray beam in all direction. The scattered X-ray must be in phase to the incident beam for the diffraction maxima to occur. For cento-symmetric crystal, the phase of the scattered peak can only be *0* or π. The discrete parallel planes in crystal; separated by distance *d* will reflect the X-ray beam. To give rise to a diffraction or scattering peak, reflection of X-ray by the different planes in the crystal needs to be a constructive interference, meaning that they must arrive at the detector in phase. Hence, the path difference between them must be an integer number of the X-ray wavelength λ as described in Equation 2.1. The diffraction pattern is related to the reciprocal lattice of the lattice planes *h*, *k*, *l*. The sample to detector distance is calculated by calibrating the system with silver behenate, a known calibrant with characteristic *d*-spacing (58.38 Å). From this calculation, the *d*-spacing of the samples can be determined (Tyler et al., 2015).

Sample Preparation

The dry samples were grinded with mortar and pestle and then packed into the paste cell sample holder. The samples were then heated to their respective isotropic temperature

and cooled to room temperature and left overnight in vacuum for equilibration. The SAXS analysis is performed on the next day or after the sample had reached equilibration.

The hydrated samples were prepared at various water concentration by addition of appropriate amount of deionised water with dry lipids into the 2 mL microcentrifuge tube. The samples were then homogenised by repeated heating (to 60 °C) and cooling (to room temperature) followed by centrifugation. The homogenised samples were then allowed to equilibrate for at least a fortnight prior to SAXS measurement. Approximately, 50 mg of sample was transferred to a paste cell holder and loaded into the X-ray machine.

Measurement

The dry and hydrated samples were characterised using the analytical SAXS from SAXSess, Anton Paar Austria. The instrument was equipped with an X-ray tube (DX-Cu 12x0.45, SERFERT) generating Cu-K_α with wavelength λ = 1.542 Å at 40 kV and 50 mA. The measurements were performed under line collimation in vacuum. The sample to detector distance was 317 mm and the scattering patterns were recorded using one-dimensional diode detector. Silver behenate was used as the calibrant in all measurements. The temperature of the samples was controlled using the Peltier system utilising TCStage 300 within an accuracy of ±0.1 °C. During measurements, both dry and hydrated samples were left to equilibrate in the Peltier system for at least 30 minutes at the desired operating temperature prior to the 1-hour frame acquisition time. The acquired data was calibrated by normalising the primary beam using the SAXStreat software. Space group assignment of the liquid crystal phases and its corresponding lattice parameters were determined using the SGI software (Space Group Indexing, V.03.2012) (Liew, 2016; Liew et al., 2015; Salim et al., 2016).

Binary Phase Diagram

Glycolipids-water mixtures were prepared by weighing out small amount of dry lipid (approximately 40 mg) into glass tubes, followed by addition of water. The samples were prepared in the range of 5% (w/w) to 90% (w/w) with 2 to 3% (w/w) water content intervals. The tubes were then flame-sealed, and the lipid-water mixtures were homogenised by centrifugation and heating-cycled for several times. The sample tubes were placed in the water bath at temperature 25 °C, 35 °C, 45 °C and 60 °C and left to equilibrate for one hour at each temperature. The samples were then examined by visual inspection between crossed polarisers (Nilsson et al., 1997; Zahid et al., 2013). The pseudo binary phase diagram is constructed and a few concentrations were selected for phase verification using SAXS.

CHAPTER 3 : RESULTS AND DISCUSSION

The following chapter presents the results and discussion of the present study. In this work, five branched-chain maltosides with variations on the length of the hydrophobic tail attached to the maltose head group were successfully synthesised. The thermotropic and lyotropic liquid crystalline phases of these compounds were characterised with DSC, OPM and SAXS.

3.1 Synthesis of Guerbet Maltosides

Using the synthesis method described in Chapter 2, five alkyl branched-chain maltosides were obtained. The compounds annotation and NMR data of the Guerbet maltosides are given in the following pages. The NMR spectra for the acetate compounds are provided in Appendix C. The β-anomeric purity was confirmed with the appearance of doublet peaks in the ^{1}H-NMR spectra for all compounds at approximately 4.26 ppm with coupling constant value around 7.60 Hz corresponding to the trans coupling between H at C_1 and the H at C_2 (Hassan, 2001) and also the absence of doublet peak corresponding to the α-anomer at 4.7 ppm (Patrick et al., 2018). The yield of the reactions is tabulated in **Table 3.1**. The acetate sugar compounds gave white solid powder appearance while the hydroxy sugar compounds gave white flaky powder appearance and very hygroscopic in nature.

Table 3.1: The molecular formula and the yield of the Guerbet maltosides before and after deacetylation.

Compound	Before deacetylation		After deacetylation	
	Molecular formula	Starting material (g)	Molecular formula	Yield (g)
β-Mal-C_6C_2	$C_{34}H_{52}O_{18}$	2.0	$C_{20}H_{38}O_{11}$	1.6
β-Mal-C_8C_4	$C_{38}H_{60}O_{18}$	2.2	$C_{24}H_{46}O_{11}$	1.8
β-Mal-$C_{10}C_6$	$C_{42}H_{68}O_{18}$	2.4	$C_{28}H_{54}O_{11}$	2.0
β-Mal-$C_{12}C_8$	$C_{46}H_{76}O_{18}$	2.6	$C_{32}H_{62}O_{11}$	2.2
β-Mal-$C_{14}C_{10}$	$C_{50}H_{84}O_{18}$	2.8	$C_{36}H_{70}O_{11}$	2.4

2-ethyl-hexyl-*β*-D-maltoside, ***β*-Mal-C$_6$C$_2$**

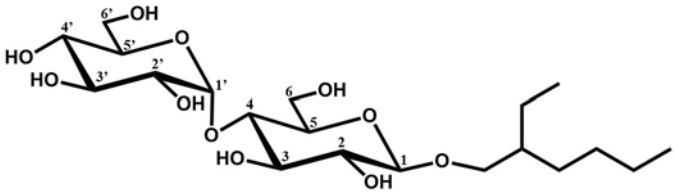

^{1}H-NMR (400 MHz, CD_3OD): δ (ppm) = 5.18 (d, 1H, $J_{1',2'}$ = 3.6 Hz, H-1'), 4.26 (d, 1H, $J_{1,2}$ = 7.6 Hz, H-1), 3.91 (dd, 1H, $J_{6a,6b}$ = 12.0 Hz, H-6a), 3.81–3.87 (m, 3H, H-4', H-6b, H-6a'), 3.67–3.73 (m, 2H, H-5', H-6b'), 3.58–3.65 (m, 2H, H-3, H-3'), 3.55 (dd, 1H, $J_{3,4}$ = 8.8 Hz, H-4), 3.36–3.48 (m, 3H, H-2', H-5, H-2), 3.23–3.34 (m, 2H, OCH_2), 1.56 (m, 1H, CH), 1.33–1.48 (m, 8H, CH_2), 0.92 (t, 6H, J = 6.8 Hz, 2 x CH_3).

^{13}C-NMR (100 MHz, CD_3OD): δ (ppm) = 103.4 (C-1'), 101.5 (C-1), 79.9 (C-2), 76.5 (C-3'), 75.2 (C-3), 73.7 (C-2'), 73.4 (C-5'), 72.8 (C-5), 72.3 (OCH_2), 70.1 (C-4', C-4), 61.4 (C-6'), 60.7 (C-6), 39.7 (CH), 22.7–30.1 (CH_2), 13.1, 10.0 (CH_3).

2-butyl-octyl-*β*-D-maltoside, ***β*-Mal-C$_8$C$_4$**

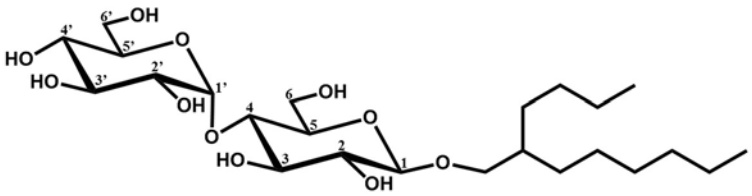

^{1}H-NMR (400 MHz, CD_3OD): δ (ppm) = 5.18 (d, 1H, $J_{1',2'}$ = 3.6 Hz, H-1'), 4.26 (d, 1H, $J_{1,2}$ = 7.6 Hz, H-1), 3.91 (dd, 1H, $J_{6a,6b}$ = 12.2 Hz, H-6a), 3.81–3.86 (m, 3H, H-4', H-6b, H-6a'), 3.67–3.73 (m, 2H, H-5', H-6b'), 3.58–3.65 (m, 2H, H-3, H-3'), 3.55 (dd, 1H, $J_{3,4}$ = 8.8 Hz, H-4), 3.36–3.48 (m, 3H, H-2', H-5, H-2), 3.23–3.36 (m, 2H, OCH_2), 1.62 (m, 1H, CH), 1.32–1.44 (m, 16H, CH_2), 0.92 (t, 6H, J = 6.8 Hz, 2 x CH_3).

^{13}C-NMR (100 MHz, CD_3OD): δ (ppm) = 103.3 (C-1'), 101.5 (C-1), 79.9 (C-2), 76.5 (C-3'), 75.2 (C-3), 73.7 (C-2'), 73.4 (C-5'), 72.8 (C-5), 72.7 (OCH_2), 70.1 (C-4', C-4), 61.4 (C-6'), 60.8 (C-6), 38.2 (CH), 22.3–31.7 (CH_2), 13.1 (CH_3).

2-hexyl-decyl-*β*-D-maltoside, ***β*-Mal-C$_{10}$C$_6$**

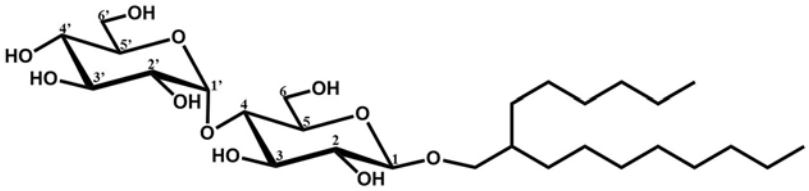

^{1}H-NMR (400 MHz, CD_3OD): δ (ppm) = 5.18 (d, 1H, $J_{1',2'}$ = 3.6 Hz, H-1'), 4.26 (d, 1H, $J_{1,2}$ = 8.0 Hz, H-1), 3.91 (dd, 1H, $J_{6a,6b}$ = 12.0 Hz, H-6a), 3.81–3.86 (m, 3H, H-4', H-6b, H-6a'), 3.67–3.73 (m, 2H, H-5', H-6b'), 3.58–3.65 (m, 2H, H-3, H-3'), 3.55 (dd, 1H, $J_{3,4}$ = 9.2 Hz, H-4), 3.36–3.48 (m, 3H, H-2', H-5, H-2), 3.23–3.36 (m, 2H, OCH_2), 1.63 (m, 1H, CH), 1.32–1.43 (m, 24H, CH_2), 0.92 (t, 6H, J = 6.8 Hz, 2 x CH_3).

^{13}C-NMR (100 MHz, CD_3OD): δ (ppm) = 103.3 (C-1'), 101.5 (C-1), 79.9 (C-2), 76.5 (C-3'), 75.2 (C-3), 73.7 (C-2'), 73.4 (C-5'), 72.8 (C-5), 72.7 (OCH_2), 70.1 (C-4', C-4), 61.4 (C-6'), 60.8 (C-6), 38.1 (CH), 22.3–31.7 (CH_2), 13.1 (CH_3).

2-octyl-dodecyl-*β*-D-maltoside, ***β*-Mal-C$_{12}$C$_8$**

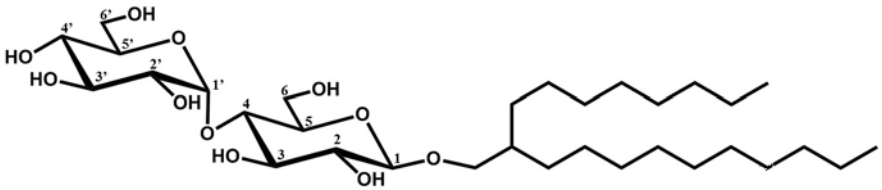

^{1}H-NMR (400 MHz, CD_3OD): δ (ppm) = 5.18 (d, 1H, $J_{1',2'}$ = 3.6 Hz, H-1'), 4.26 (d, 1H, $J_{1,2}$ = 7.6 Hz, H-1), 3.91 (dd, 1H, $J_{6a,6b}$ = 12.0 Hz, H-6a), 3.81–3.86 (m, 3H, H-4', H-6b, H-6a'), 3.67–3.73 (m, 2H, H-5', H-6b'), 3.58–3.66 (m, 2H, H-3, H-3'), 3.55 (dd, 1H, $J_{3,4}$ = 9.2 Hz, H-4), 3.36–3.48 (m, 3H, H-2', H-5, H-2), 3.23–3.36 (m, 2H, OCH_2), 1.63 (m, 1H, CH), 1.32–1.43 (m, 32H, CH_2), 0.92 (t, 6H, J = 6.8 Hz, 2 x CH_3).

^{13}C-NMR (100 MHz, CD_3OD): δ (ppm) = 103.3 (C-1'), 101.5 (C-1), 79.9 (C-2), 76.5 (C-3'), 75.2 (C-3), 73.7 (C-2'), 73.4 (C-5'), 72.8 (C-5), 72.7 (OCH_2), 70.1 (C-4', C-4), 61.4 (C-6'), 60.8 (C-6), 38.1 (CH), 22.4–31.7 (CH_2), 13.1 (CH_3).

2-decyl-tetradecyl-β-D-maltoside, ***β*-Mal-$C_{14}C_{10}$**

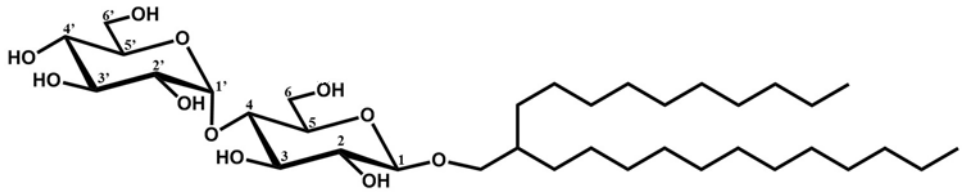

^{1}H-NMR (400 MHz, CD_3OD): δ (ppm) = 5.18 (d, 1H, $J_{1',2'}$ = 3.6 Hz, H-1'), 4.26 (d, 1H, $J_{1,2}$ = 7.6 Hz, H-1), 3.88 (dd, 1H, $J_{6a,6b}$ = 12.0 Hz, H-6a), 3.81–3.83 (m, 3H, H-4', H-6b, H-6a'), 3.67–3.73 (m, 2H, H-5', H-6b'), 3.58–3.66 (m, 2H, H-3, H-3'), 3.55 (dd, 1H, $J_{3,4}$ = 9.2 Hz, H-4), 3.37–3.48 (m, 3H, H-2', H-5, H-2), 3.23–3.33 (m, 2H, OCH_2), 1.63 (m, 1H, CH), 1.32–1.44 (m, 40H, CH_2), 0.92 (t, 6H, J = 6.8 Hz, 2 x CH_3).

^{13}C-NMR (100 MHz, CD_3OD): δ (ppm) = 103.3 (C-1'), 101.5 (C-1), 79.9 (C-2), 76.5 (C-3'), 75.2 (C-3), 73.7 (C-2'), 73.4 (C-5'), 72.8 (C-5), 72.7 (OCH_2), 70.2 (C-4', C-4), 61.4 (C-6'), 60.8 (C-6), 38.1 (CH), 22.3–31.7 (CH_2), 13.1 (CH_3).

Thermal behaviour of the hygroscopic alkylmaltosides are highly dependent on the degree of hydration (Ericsson et al., 2005). To remove moisture, the compounds are dried under vacuum over phosphorus pentoxide for at least 48 hours prior to any thermotropic measurement. FTIR spectra of β-Mal-$C_{14}C_{10}$ (Figure 3.1) shows that H_2O vibrational peak intensity at approximately 1643 cm^{-1} lessened considerably with drying in relative to the compound left at ambient and in excess water. Furthermore, the presence of symmetric stretching vibration peak of methylene groups from the alkyl chain in the range of 2853 to 2854 cm^{-1} in all the studied compounds indicates the presence of liquid crystalline phase (Garidel et al., 2015).

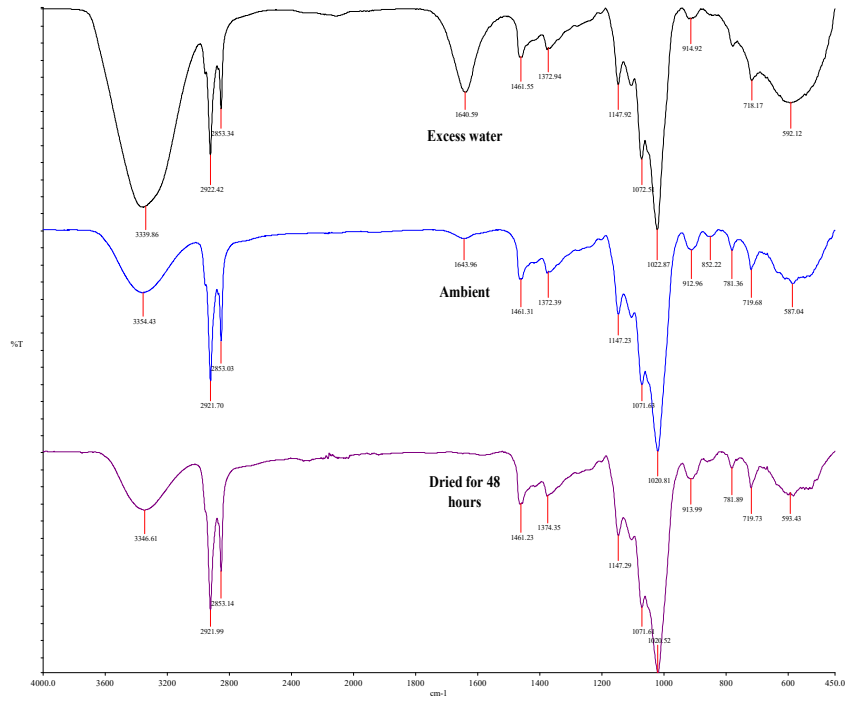

Figure 3.1: FTIR spectra for *β*-Mal-C14C10 in dry (after lyophilised in vacuum oven for at least 48 hours), left in ambient moisture for 96 hours and in excess water form.

3.2 Differential Scanning Calorimetry

All the DSC data are presented in Table 3.2 and Figure 3.2. The DSC thermograms showed the typical endothermic clearing transition into the isotropic phase. Step-shaped peaks associated with the glass transition, T_g were observed instead of the melting transition peaks.

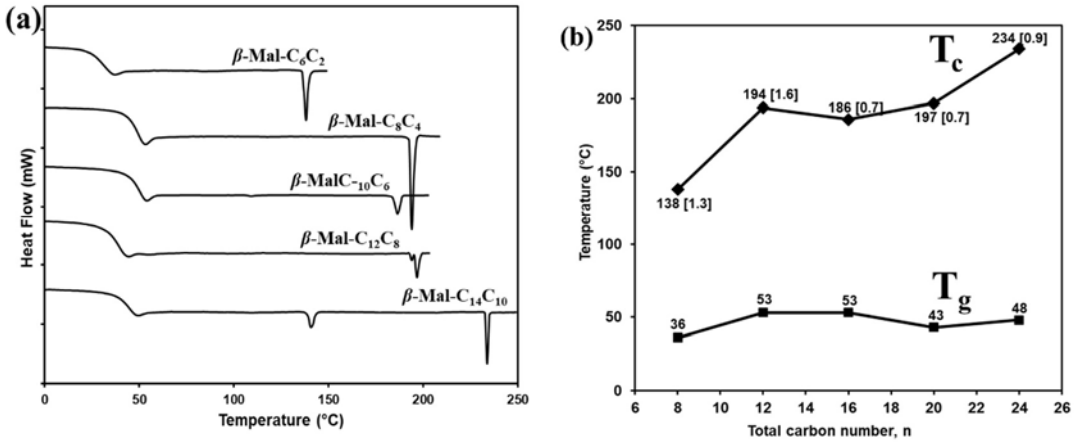

Figure 3.2: (a) DSC thermograms (with baseline correction) of dry *β*-D-maltosides with heating scan rate of 5 °C/min; (b) T_g and T_c trends for the Guerbet maltosides.

The glass transitions of these maltosides were detected between 35 to 53 °C. A glass is an amorphous solid which does not possess long-range translational order (Elliott, 1990) and it can be obtained either from the heating or cooling scans (Kocherbitov & Söderman, 2004; Ogawa et al., 2013). For example, on cooling near the glass transition, motions are restricted due to the sugar interaction which is predominantly hydrogen bonds. At the glassy point, molecules are frozen in positions they adopted just before the transition. Consequently, the structure of the newly formed glassy crystals is closer to that of liquid crystals, thus it was assigned as lamellar glass ($L_{\alpha G}$) (Kocherbitov & Söderman, 2004). The OPM texture in Figure 3.3(c) and its inset show similar textures for both lamellar at 54 °C and lamellar glass at ~27 °C. The presence of glass transition possibly supressed the melting transition into the liquid crystal phase (Sagnella et al., 2011). In this maltoside series, the effect of Guerbet chain length variation on T_g is small with no obvious trend (see Figure 3.2(b)). Similarly, Ogawa et al. also reported no obvious effect on T_g upon increasing the chain length ($6 \leq n \leq 12$) for monoalkylated glucosides (Ogawa et al., 2013). Other studies however demonstrated that T_g of monoalkylated glycosides increases as the number of sugar ring increases (Ericsson et al., 2005; Hashim et al., 2018). For instance, the T_g of dodecyl chain of *β*-glucoside (Ogawa et al., 2013), *β*-maltoside and *β*-maltotrioside (Ericsson et al., 2005) were reported to be around 12 °C, 65 °C and 100 °C respectively. These three glycosides have the same hydrocarbon tail i.e. n=12, implying that the glass transition is predominantly a function of the sugar headgroup, which is not too surprising since it is a common phenomenon in sugar (Kauzmann, 1948). For example, the glass transitions for glucose, maltose and maltotriose are 39 °C (Noel et al., 2000), 73 °C and 99 °C (Imamura et al., 2003), respectively. Moreover, a glass transition is a kinetic phenomenon which depends on the condition of the experiment, thermal history and sample preparation method (Kocherbitov & Söderman, 2004).

Table 3.2: Phase transition temperatures for anhydrous Guerbet and monoalkylated *β*-D-maltosides series determined by DSC. The total number of carbons is denoted by n. "-" signifies undetected value. $T_{lc \rightarrow lc}$ indicates a liquid crystal to liquid crystal transition temperature. Error in temperature is ±1 °C while error in enthalpy is ±0.1 kJ/mol.

Guerbet Maltosides	n	Transition temperature (°C) [ΔH (kJ/mol)]		
		T_g	$T_{lc \rightarrow lc}$	T_c
β-Mal-C_6C_2	8	36	-	138 [1.3]
β-Mal-C_8C_4	12	53	-	194 [1.6]
β-Mal-$C_{10}C_6$	16	53	-	186 [0.7]
β-Mal-$C_{12}C_8$	20	43	-	197 [0.7]
β-Mal-$C_{14}C_{10}$	24	48	141 [0.6]	234 [0.9]

Monoalkylated Maltosides	n	Transition temperature (°C)			Ref.
		T_g	T_m	T_c	
β-Mal-C_n	8	~60	88-103[a]	125[a]	(Boyd et al., 2000)
		54	-	123	(Kocherbitov & Söderman, 2004)
	10	~60	96-100[a]	207[a]	(Boyd et al., 2000)
		58	-	206	(Kocherbitov & Söderman, 2004)
	12	~60	102	245[a]	(Boyd et al., 2000)
			102[a]	245[a]	(von Minden et al., 2000)
		70[b]	103[a]	-[c]	(Auvray et al., 2001)
		65	-	244	(Ericsson et al., 2005)
		-	80[a]	244[a]	(Vill et al., 1989)
	14	-	107[a]	264[a]	(von Minden et al., 2000)
		-	5[a]	264[a]	(Vill et al., 1989)
		-	105	263	(Ericsson et al., 2005)
	16	-	105	-[d]	(Ericsson et al., 2005)
	18	-	106[a]	274[a]	(von Minden et al., 2000)

n.b. [a] data from OPM. [b] data from SAXS. [c] compounds darkened and decomposed at ~150 °C, hence T_c was not detected (Auvray et al., 2001). [d] Not reported in the original paper (Ericsson et al., 2005).

For comparison, the thermal behaviour of a selected monoalkylated maltosides homologous series is given in Table 3.2. The shorter-chain maltosides ($8 \leq n \leq 12$) form a glass phase upon lyophilisation and no T_g was observed for those with long alkyl chains ($n>12$). However, Ericsson et al. reported that glassy state is still possible for β-Mal-C_{14} by the means of cooling the liquid crystalline phase to room temperature and equilibration (Ericsson et al., 2005). For the same total carbon number of alkyl chain, the T_g for Guebert maltosides are lower than those of the monoalkylated maltosides. Thus, the chain branching effectively lowers the T_g. This observation is reasonable since intuitively chain branching increases the hydrophobic region making the sugar head more mobile compared to the monoalkylated systems. A computer simulation study of thermotropic monoalkylated and branched maltosides by Achari et al. supported this observation since the average autocorrelation time for the sugar head is larger for the former compared than the latter (Manickam Achari et al., 2014).

On further heating above the T_g, the DSC thermograms of Guerbet maltosides do not give any melting peak. On the contrary, the homologous series of monoalkylated maltosides from various literatures recorded melting transitions as shown in Table 3.2. From these literatures, it is not obvious if these maltosides give a recrystallisation exothermic peak (after the glass transition) as reported by Ogawa et al. for undecyl and dodecyl β-glucosides (Ogawa et al., 2013).

From Table 3.2 and Figure 3.2(a), β-Mal-C_6C_2 and β-Mal-C_8C_4 turn to isotropic at 138 °C (ΔH = 1.3 kJ/mol) and 194 °C with ΔH = 1.6 kJ/mol respectively. While the next three compounds have the clearing temperatures of 186 °C (ΔH = 0.7 kJ/mol), 197 °C (ΔH = 0.7 kJ/mol) and 234 °C (ΔH = 0.9 kJ/mol) respectively. However, their enthalpies are relatively smaller compared to the shorter chain analogues, implying the former are involved in more bond breaking compared to the latter. Interestingly, this discriminating behaviour between the first two members and the three longer chain members, is also

observed in the Guerbet xylosides (Liew et al., 2015) and mannosides (Patrick et al., 2018). In addition, thermogram of β-Mal-$C_{14}C_{10}$ shows an extra small endothermic peak at 141 °C with an enthalpy of ΔH = 0.6 kJ/mol, corresponding to a phase transition between cubic to hexagonal phase which will be confirmed by OPM. This additional transition has a relatively less enthalpy changes than main phase transition i.e. the isotropic transition which peaked at 234 °C with ΔH = 0.9 kJ/mol.

Elongation of the alkyl chain usually increases the T_c as observed in straight chain alkylmaltosides (Table 3.2). This is anticipated in increasing the chain length as more energy is required to break interactions to form the isotropic phase. However, this increase reaches a maximum point, beyond which T_c decreases. For monosaccharides, the maxima occur between 12 to 14 carbon lengths (Auvray et al., 2001), while for disaccharides headgroup i.e. maltose, such trend may be observed at a longer chain length (n > 18) (Vill et al., 1989). With the exception of β-Mal-C_8C_4, the T_c increases with increasing chain length due to the higher van der Waals interaction between the hydrophobic tails with an increase in the alkyl chain length. However, such trend was not apparent for monosaccharide Guerbet glycolipids with galactose, glucose and xylose head groups (Brooks et al., 2011; Hashim et al., 2006; Liew et al., 2015). These disaccharide lipids are expected to have higher T_c compared to the monosaccharides since the former have higher number of hydrogen bonds.

Upon comparison with the linear chain counterpart, the branching effectively decreases the T_c resulting in wider range of liquid crystalline phase due to an increased in the hydrophobic volume that may disrupt the molecular packing of the molecules (Boyd et al., 2000). Similar observation is made when a double bond is present as exhibited by *cis*-9-octadecenyl-β-D-maltopyranoside (β-Mal-$C_{18:1}$). von Minden et al. reported T_c of β-Mal-$C_{18:1}$ to be reduced by 7 °C to 267 °C when compared to β-Mal-C_{18} which undergo isotropisation at 274 °C. Moreover, increasing the number of head group

will increase the chance of hydrogen bonding in the molecules resulting in higher T_c. This is not observed however in dodecyl-*β*-D-maltotrioside (T_c = 228 °C), which has, when compared with dodecyl-*β*-D-maltoside (T_c = 244–245 °C), an extra glucose unit in the head group region. Although rather surprising, it shows that T_c is not solely governed by the number of hydroxy groups.

3.3 Optical Polarising Microscopy

The mesomorphic behaviours of dry and hydrated lipids as a function of temperature were further studied by OPM to identify the isotropic and anisotropic properties of these systems. The textures observed using optical polarising microscope can be generally divided into two types; isotropic or birefringence. Compounds that exhibit isotropic structures corresponding to phases such as micellar and cubic while those with birefringence features may give vibrant images, colour and various textures. Among the phases that exhibit birefringence are lamellar and hexagonal. Lamellar and hexagonal phases' textures can be cross-examined through various literatures while the cubic phase manifestation in the compounds is not easily distinguish due to their isotropic texture. In cubic phase, all molecules are ordered in *body-centered* or *face-centered* cubic lattice, where the light passing through the sample is refracted in every possible direction, leading to the isotropic appearance. Hence, cubic phases are best observed during the transition from a non-isotropic phase (Noel et al., 2000). One of the key characteristics of cubic phase is its high viscosity and this feature may be utilised for the phase detection (Zahid, 2013). The thermotropic phase transition temperature by OPM was determined by heating the sample and the texture observed from the optical polarising microscope was recorded during second cooling cycle. The lyotropic phase behaviour was studied by water contact penetration leading to observation of the complete phase sequence over the whole range of water concentration.

Typical OPM textures for the Guerbet maltosides are shown in Figure 3.3–3.5. The OPM results are in good agreement with those from DSC. On heating, dry β-Mal-C_6C_2 turns to isotropic at 140 °C, which is comparable to that determined by DSC. Upon cooling, the sample gives the fan-shaped texture that start to appear at 139 °C which correspond to that of lamellar (L_α) phase. Addition of water (under contact penetration) to the neat surfactant of the dry β-Mal-C_6C_2 at the room temperature reveals non-birefringence texture indicating the micellar solution (L_1) structure. Similar to the first compound, neat β-Mal-C_8C_4 exhibits the fan-shaped texture upon cooling suggesting the L_α phase formation with T_c = 195 °C. In lyotropic study, the compound forms an isotropic phase at higher water concentration as indicated by the arrow in Figure 3.3(d) followed by a stronger birefringence of L_α phase structure when the water content was gradually decreased. Similarly, the maltese cross texture observed in β-Mal-$C_{10}C_6$ upon cooling confirms the presence of L_α phase in the dry samples with T_c of 190 °C. On cooling, a rarely observed oily streaks appearance where birefringent bands are formed across a pseudo-isotropic region is obtained. The texture remains at room temperature as shown in Figure 3.3(e). The presence of maltese cross structure in Figure 3.3(e) indicates the formation of L_α phase in the samples and SAXS investigations in later section confirms the existence of this phase. The same L_α texture persisted in the presence of water (Figure 3.3(f)). It was reported that lamellar amphiphilic phases form pseudo-isotropic textures with oily streaks (Saupe, 1977).

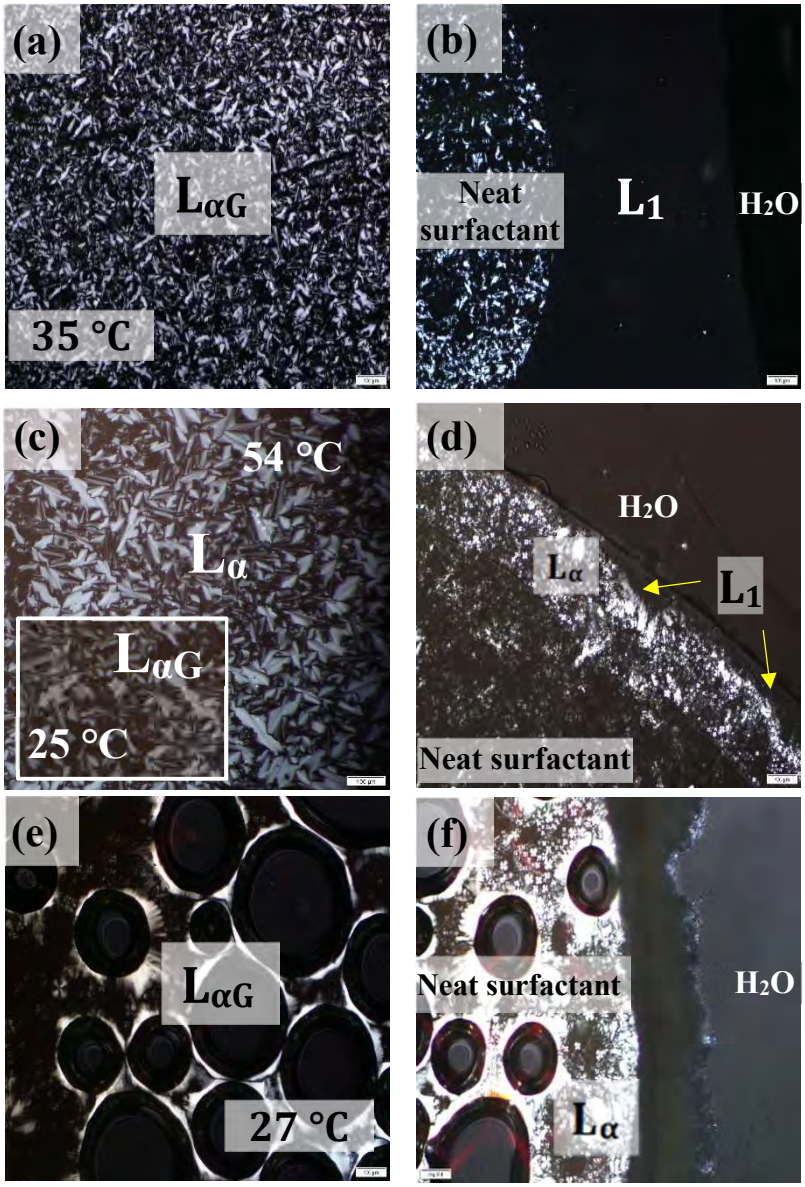

Figure 3.3: OPM texture of: (a) L_α of dry *β*-Mal-C_6C_2 (x10); (b) micellar solution, L_1 of *β*-Mal-C_6C_2 after contact with water (x10); (c) fan-shaped texture of L_α in dry *β*-Mal-C_8C_4 (x10). The inset shows the glassy lamellar phase at the room temperature; (d) isotropic and birefringence textures observed from *β*-Mal-C_8C_4 after contact preparation scan; (e) coexistence of a maltese cross texture indicating L_α phase and a pseudo-isotropic region of dry *β*-Mal-$C_{10}C_6$; (f) maltese cross structure and pseudo-isotropic region remain in *β*-Mal-$C_{10}C_6$ upon addition of water. All the lyotropic textures were captured at the room temperature.

The fourth analogue, *β*-Mal-$C_{12}C_8$ in anhydrous state turns to isotropic liquid at 196 °C. Upon cooling, it exhibited unusual birefringent texture between the first and second cooling. A mosaic structure was observed during first cooling (Figure 3.4(a)) whereas a striated texture (Figure 3.4(b)) was perceived upon second cooling. The OPM textures are rather uncommon of a sugar lipid and is quite distinct from the focal conic and

fan-shaped texture. The rare anisotropic textures are not clear to allow for an unambiguous identification of the liquid crystalline phases, as it could be lamellar, hexagonand, cubic or a mixture of these. Although a proper phase identification could be performed by SAXS, it was later prevailed (in next section) that this is also not the case for this compound. Figure 3.4(c) shows a stronger birefringence texture was obtained at higher water concentration with the occurrence of myelin structure. The observation signifies the formation of a L_α phase in this compound.

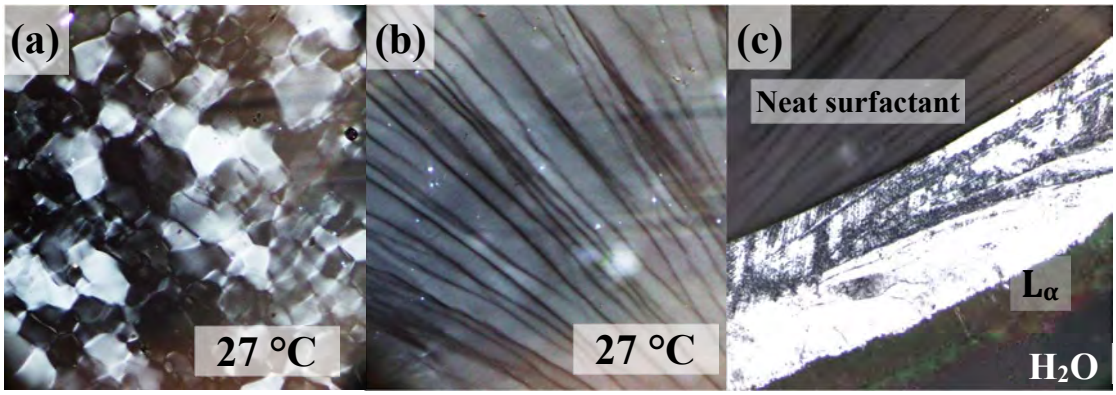

Figure 3.4: OPM micrograph for dry *β*-Mal-$C_{12}C_8$ gives different texture upon repeated heating and cooling cycle. (a) The mosaic structure upon first cooling and (b) striated texture upon second cooling. The hydrated *β*-Mal-$C_{12}C_8$ gives L_α structure at high water concentration gradient as shown in (c).

The longest chain member *β*-Mal-$C_{14}C_{10}$ exhibits polymorphism behaviour as predicted from the DSC results. As shown in Figure 3.4, the sample form the L_α phase at room temperature before turning to a non-birefringence (isotropic) phase at temperature 117 °C. This isotropic phase is presumed to be the cubic phase whose identity shall be confirmed by SAXS. The weak birefringence texture along with the transition bars observed in Figure 3.4(b) signifies the phase transformation from a lamellar to a cubic phase. Additional heating of the isotropic phase gave a birefringence phase of fan-shaped texture of inverse hexagonal (H_2) phase at 136 °C, which is comparable to the DSC result (see Figure 3.2 and Table 3.2). However, the DSC thermogram did not give the phase transition peak from the L_α to cubic, since $L_\alpha \leftrightarrow$ cubic interconversion is kinetically controlled (Noel et al., 2000). Further increase in temperature led to the T_c at 238 °C.

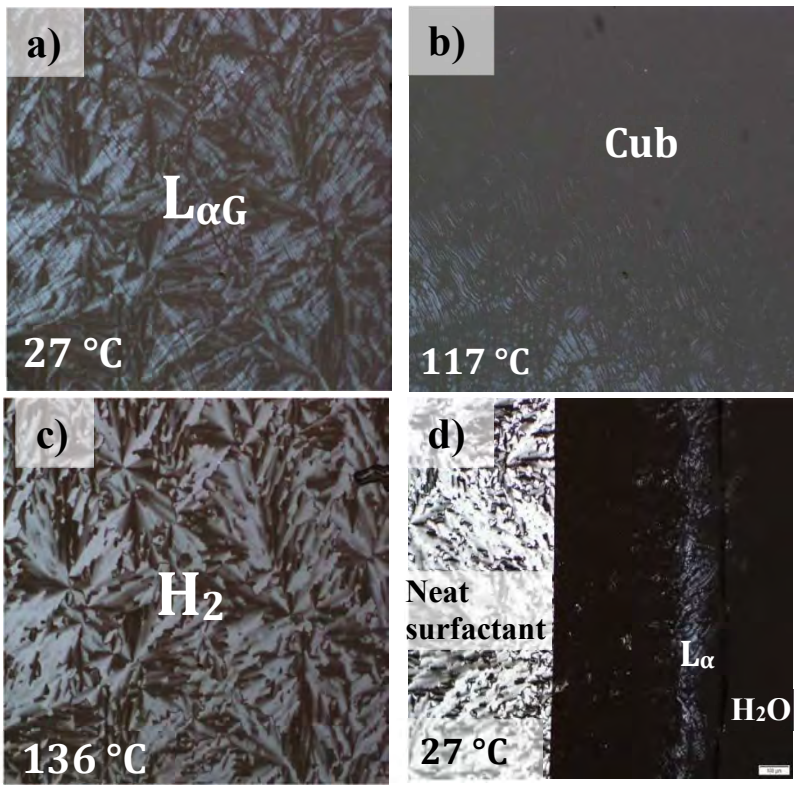

Figure 3.5: Polymorphism of *β*-Mal-$C_{14}C_{10}$ was observed in OPM texture: (a) L_α structure of dry *β*-Mal-$C_{14}C_{10}$ at 51.5 °C; (b) cubic phase of dry *β*-Mal-$C_{14}C_{10}$ at temperature 117.3 °C; (c) fan-shaped texture of H_2 in dry *β*-Mal-$C_{14}C_{10}$ at temperature 136.0 °C and (d) myelin texture of *β*-Mal-$C_{14}C_{10}$ after water penetration scan.

These observations can be explained as the molecular structures are more rod-like shaped and possess the zero-mean curvature that favours the formation of L_α at the lower temperature. Upon temperature increment, the rod-shaped molecules at the L_α phase becomes more wedge-shaped due to the increase motions in the hydrocarbon chains resulting in the formation of cubic phase. Cubic phase can be regarded as a structural compromise due to the destabilisation of molecular moiety in lamellar structure. Further destabilisation results in H_2 phase as observed in *β*-Mal-$C_{14}C_{10}$ (Garidel et al., 2008; Milkereit et al., 2005). The molecular self-assembly of *β*-Mal-$C_{14}C_{10}$ is illustrated in Figure 3.6. Contact penetration scan of *β*-Mal-$C_{14}C_{10}$ reveals a myelin structure indicating the formation of L_α phase. The formation of myelin in high water concentration region has also been reported in dialkyl glycosyl bearing maltose head group (Milkereit et al., 2005).

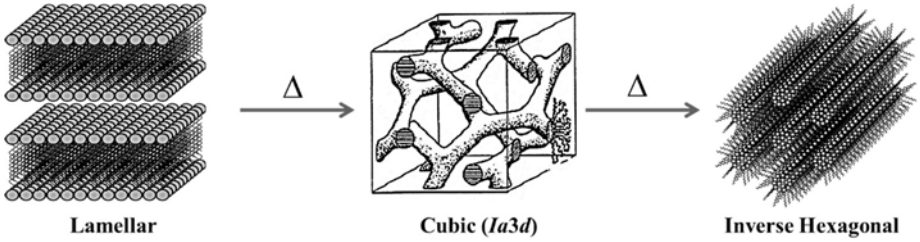

Figure 3.6: Molecular self-assembly of *β*-Mal-$C_{14}C_{10}$ during the thermal polymorphism.

Upon second cooling, no morphological changes in OPM textures were observed below and after the T_g (values from DSC) for all the compounds. When the liquid crystal undergoes a glass transition, the newly formed glassy crystal phase retains almost the same structure as in the liquid crystal and relaxes into the more ordered glassy phase rather slow. Since it takes a long time, there is no distinct phase changes occurred, hence, the textures remain the same below and after T_g (Ogawa et al., 2013).

In general, branched-chain maltosides have a wide range of L_α due to strong electrostatic interaction via hydrogen bonding in the hydrophilic region henceforth, the transformation into another non-lamellar phase may occurs at a higher chain length or temperature (Hashim et al., 2006). When two opposing factors from the head group and the hydrocarbon chain are equally dominant, the self-organisation becomes frustrated and compromised to give a thermotropic polymorphism, where the system displays a series of phases from lamellar to the non-lamellar (V_2, H_2) by heating as shown in Figure 3.4. The tendency of the hydrophilic head region to form lamellar structures and the hydrophobic region to curve result in the packing frustration which induces the formation of a cubic phase (Hashim et al., 2012). From the previous studies of Guerbet glycosides, the orientation of the C_4–OH and the glycosidic linkages modify the arrangement of hydrogen bonding in the hydrophilic region, thus influencing the thermal properties of the self-assembly (Hashim et al., 2006).

The T_c from OPM and of DSC obtained for this work are similar to within the error. Compared to previously reported (Hashim et al., 2006) phase transition temperatures, the results by OPM are lower for most compounds except for β-Mal-$C_{12}C_8$, whose T_c is a few °C different from the present study. The presence of water in the former study could be the reason of the behavioural difference since a small amount of water is sufficient to lessen the clearing point of glycolipids. This effect was also observed in 4-cyano-4'-pentylbiphenyl (5CB) dispersion system (Noh et al., 2016). The phase behaviour and transition temperature for β-Mal-$C_{12}C_8$, between the previous and current works are significantly different due to dissimilar degrees of purification in the compounds as the previous work reported that the β-Mal-$C_{12}C_8$ contained 5% α-anomer (Hashim et al., 2006). It is widely accepted that the anomeric purity in glycosides considerably affect the mesomorphic behaviour (von Minden et al., 2000; Zahid et al., 2013).

Nature of the head group largely governs the thermal behaviour of alkylmaltosides due to the strong intermolecular hydrogen bonds between the glycolipid head groups. Thermal behaviour of the hygroscopic alkylmaltosides is extremely sensitive to sample history and presence of trace water may give a particularly drastic effect (Ericsson et al., 2005). From the results obtained, it was suggested that the head group and interfacial hydration determine the thermotropic and lyotropic phase properties. The interaction between head group interface and water molecules determines the formation of lamellar phase. In lyotropic studies, the number of phases, the rate of formation and the molecular packing of the phases are also determined by these interactions.

3.4 Small-Angle X-Ray Scattering

Thermotropic study

SAXS studies of the first three anhydrous maltosides i.e. β-Mal-C_6C_2, β-Mal-C_8C_4 and β-Mal-$C_{10}C_6$ (Figure 3.7(a–c)) reveal a typical L_α phase pattern which is characterised by the reflections [100], [200] and [300]. Their lattice parameters are 28.0 Å, 29.0 Å and 31.6 Å respectively. These results confirmed the observations of the L_α phase under an optical polarising microscope for these compounds. The chain length effect for these shorter Guerbet chains is insufficient to counter the strong influence of the bulky maltose head groups which support the formation of the lamellar layers. This is due to the molecular balance between the hydrophobic chain moiety bound to the ether bond with the maltose head group give a more rode-like packing with equivalent balance between these two parts, hence the formation of lamellar phase is more favoured (Liew, 2016).

Upon increasing the hydrophobic chain length, the properties of the glycolipids are dominated by the hydrocarbon chain melting process as the lipophilic chains are said to be the main drive for the phase transition. The striated birefringent texture from OPM study predicts the formation of either L_α or H_2 phase in anhydrous β-Mal-$C_{12}C_8$. However, the SAXS pattern of this lipid gave unusual characteristic peaks which is different from the reflection order of a L_α or H_2 phases (see Figure 3.7(d)). This phase is characterised by a scattering pattern containing about 12 sharp lines below 0.6 $Å^{-1}$. The WAXS study (Figure 3.8(b)) identifies this as a liquid crystal phase based on a broad diffuse peak close to 4.7 Å. Hitherto, the identity of β-Mal-$C_{12}C_8$ mesophase was unassignable to any specific lattice and its complex SAXS pattern obtained upon an overnight cooling from heating to its isotropic phase indicates a possible involvement of kinetic retardations. The results may imply that the compound is kinetically unstable since its SAXS peaks appeared to be shifting with time after left to equilibrate for a week as shown in Figure

3.8(d). Hence, the sample is said to be kinetically metastable and may require longer equilibration time for it to return to its original phase. This metastable phase can exist over long time so that no spontaneous conversion to the ground state occurs in sensible time. The lack of reversibility in lipid phase transitions which is indicated by the occurrence of distinct metastable phases may be attributed to:

(1) long hydration/dehydration times,
(2) slow reformation of hydrogen bond networks,
(3) necessity of large spatial rearrangements in lamellar/non-lamellar transition, and
(4) relative stability of the interfaces between rigid and fluid domains.

Such behaviour has been observed in cooling scans of phospholipid and glycolipid dispersion (Tenchov, 1991). The heating scan for these compounds are further investigated using SAXS by varying the temperature and the scattering peaks are depicted as shown in Figure 3.8(e). As observed in Figure 3.8(e), the compound remains metastable in a wide range of temperature resulting in difficult peaks assignment for phase determination. It was proposed that two cubic mesophases may co-existing in this particular compound, however the assignment could not be confirmed as observed in the phase assignment of previous studies (Hashim et al., 2006) and the comparison between the current and previous study was tabulated in Table 3.3.

From previous study (Hashim et al., 2006), β-Mal-$C_{12}C_8$ was assigned with cubic phase of space group *Im*3*m* and *Pn*3*m* from SAXS measurement and β-Mal-$C_{14}C_{10}$ displayed the *Pn*3*m* cubic space group. These discrepancies with the present study may be due to the difference in purity and hydration factors.

Table 3.3: Comparisons of phase transition temperature in DSC (°C) and the liquid crystalline phases observed in SAXS of the *β*-D-Maltosides between a previous study (Hassan, 2001) and current study. The transition temperatures were reported from DSC and the phase determination from OPM textures.

Compound	Previous study		Present study	
	DSC	SAXS	DSC	SAXS
β-Mal-C_6C_2	SmA 136.9 Iso	SmA	$L_{\alpha G}$ 138 Iso	L_α
β-Mal-C_8C_4	SmA 189.9 Iso	SmA	$L_{\alpha G}$ 194 Iso	L_α
β-MalC-$_{10}C_6$	SmA 189.6 Iso	SmA	$L_{\alpha G}$ 186 Iso	L_α
β-Mal-$C_{12}C_8$	Cr 19.1 SmA 117.1 Cub 175.2 Col 213.0 Iso	*Im*3*m*, *Pn*3*m*	$L_{\alpha G}$ 197 Iso	metastable
β-Mal-$C_{14}C_{10}$	Cr 18.8 SmA 69 Cub, 136.7 Col (?) Iso	*Pn*3*m*	$L_{\alpha G}$ 141 H_2 234 Iso	*Ia*3*d*

n.b. Previous study (Hashim et al., 2006) denotes L_α as Smectic A (SmA) and H_2 is symbolised as Col.

Finally, Figure 3.7(e) depicts the scattering pattern of *β*-Mal-$C_{14}C_{10}$ at 25 °C which consists of [211], [220], [321] and [400] reflections. These Miller indices unveils an inverse bicontinuous cubic structure of space group *Ia*3*d* with lattice parameter of 89.7 Å. The assignment of this compound with inverse phase behaviour is due to the molecule possesses a large CPP (>1), as evidenced in the formation of non-lamellar V_2 phase. The observed results confirm that chain branching supports curved phases, as reported for other branching systems (Hato et al., 2009; Mannock et al., 2007; Milkereit et al., 2005). In the case of branched-chain Guerbet *β*-xylosides (Liew et al., 2015) and *β*-glucosides (Brooks et al., 2011), the non-lamellar phase can be formed by chain length as short as C_8C_4 while the maltoside counterpart requires longer chain length i.e. $C_{12}C_8$ to give curved phases which is consistent with the mean curvature theory (Shearman et al., 2006). The *β*-Mal-$C_{14}C_{10}$ showed polymorphism over a temperature scan with phase sequence as follows: $L_\alpha \leftrightarrow V_2$ (*Ia*3*d*) $\leftrightarrow H_2$. Hence, L_α phase was anticipated from the SAXS measurement at 25 °C. However, the pattern for a cubic *Ia*3*d* structure was observed upon an overnight cooling from heating to its isotropic phase. From the phase sequence, the cubic mesophase is located between the lamellar and inverse hexagonal phases. Thus, the presence of the bicontinuous cubic phase implies a remarkable metastability over an extended temperature range once formed and possibly can be reset

into the lamellar phase only by further cooling (Ericsson et al., 2005). Another possible explanation for the different observation between the OPM and SAXS measurement for this phase is due to different sample preparations in the two techniques. In the former, a small amount of sample in a thin layer was used, while in the latter, the cell contained much more sample. Large variation of kinetic origin can be induced in the lipid phase behaviour by parameters such as thermal history, scan rate and temperature gradients in the measuring cell (Tenchov, 1991).

Binary Phase Diagram

The five phase diagrams with a controlled water content ranging from approximately 5% (w/w) to 90% (w/w) are given in Figure 3.9(a–e). The temperature ranged from 25 to 60 °C. The phase boundaries as well as excess water region were obtained visually between crossed polariser sheets and are shown in the shaded areas in Figure 3.9. Selected hydrated samples are measured by SAXS to elucidate their mesophases and structural parameters following at least two weeks of equilibration at the room temperature. The measurement conducted in the heating direction as a function of temperature and composition are superimposed on the partial binary phase diagrams data. These data are denoted by different symbols representing different type of liquid crystal phases. In general, L_α phase dominates the lyotropic self-assembly of all compounds which determined from the scattering pattern in the following ratios: 1, 2, 3 (see Figure 3.7(h–j) for example) and its anisotropic behaviour between crossed polariser sheets. Additionally, the normal micellar solution L_1 has a significant region of existence at higher water content of the shorter chain length Guerbet β-D-maltosides. Its SAXS data revealed a single wide peak which indicates the absence of long-range crystalline order. The calculated lattice parameters for each phase are tabulated as a function of temperature and water content in Table 3.5.

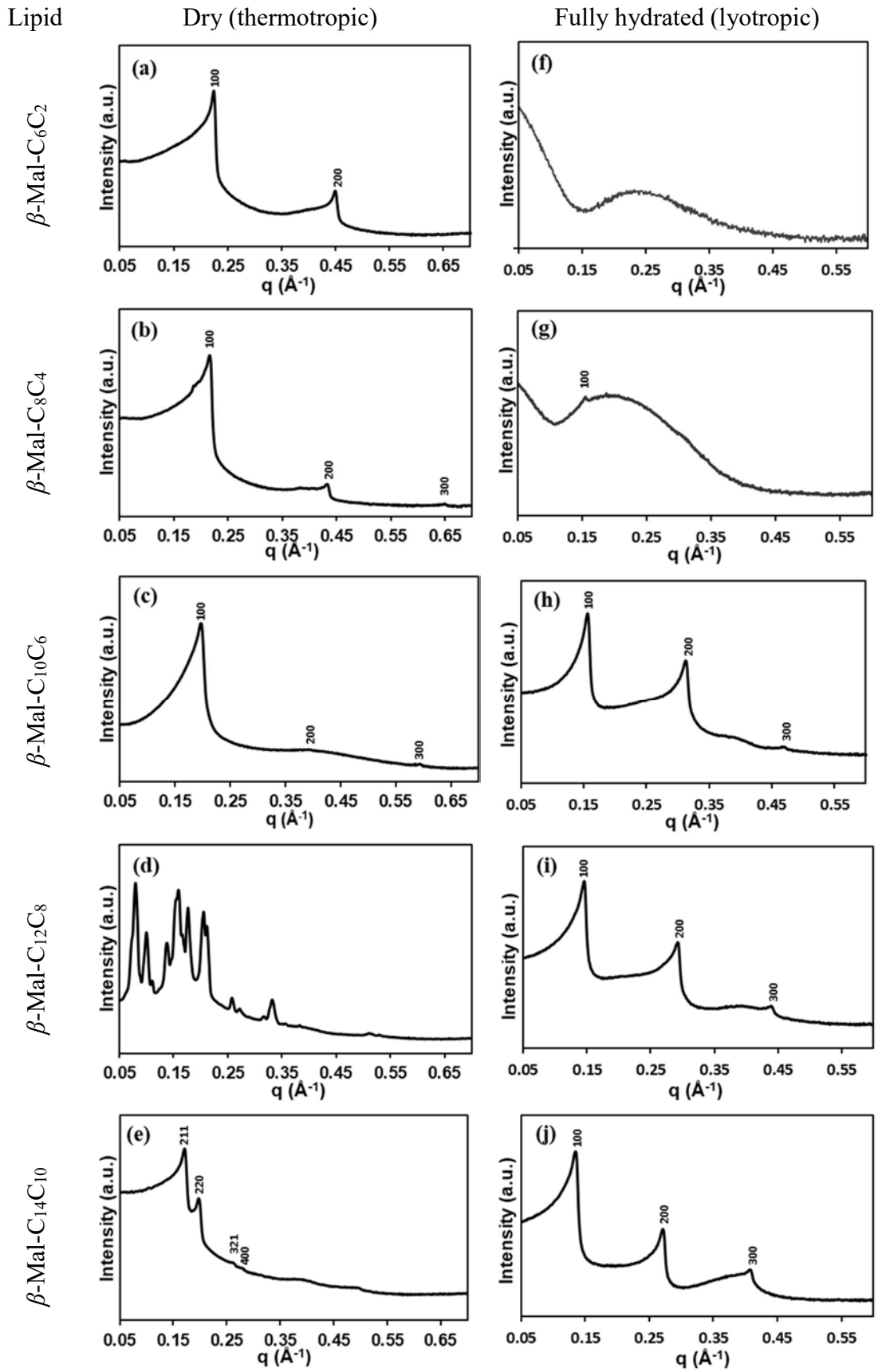

Figure 3.7: SAXS patterns of *β*-D-maltosides under dry and fully hydrated conditions at 25 °C with the following phase: (a) L_α; (b) L_α; (c) L_α; (d) unassignable phase; (e) V_2 (*Ia3d*); (f) L_1; (g) L_1 and L_α; (h) L_α; (i) L_α and (j) L_α.

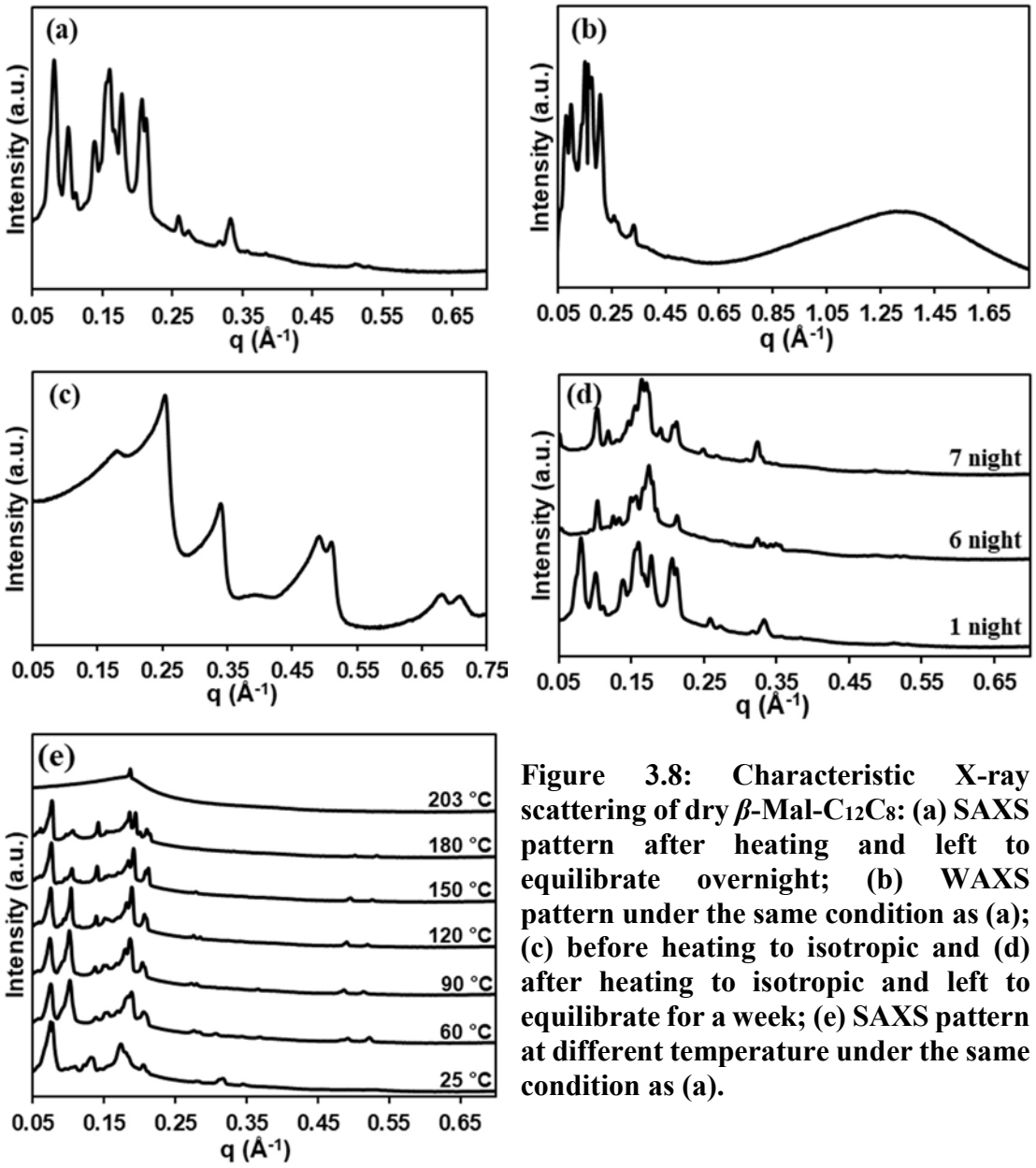

Figure 3.8: Characteristic X-ray scattering of dry *β*-Mal-$C_{12}C_8$: (a) SAXS pattern after heating and left to equilibrate overnight; (b) WAXS pattern under the same condition as (a); (c) before heating to isotropic and (d) after heating to isotropic and left to equilibrate for a week; (e) SAXS pattern at different temperature under the same condition as (a).

Figure 3.9(a) shows the partial phase diagram of *β*-Mal-C_6C_2. At low water contents up to 15% (w/w), *β*-Mal-C_6C_2/water system showed anisotropic behaviour between 25–60°C and the SAXS data at 10% (w/w) revealed the scattering pattern of the lamellar phase. A fluid isotropic region starts to form at 17.5% (w/w) and concentration beyond. Hence, this concentration was assigned as the excess water point (dashed line) for *β*-Mal-C_6C_2. SAXS measurement at 25% (w/w) reveals two broad peaks which can be associated with the lamellar phase. Nevertheless, using crossed polariser sheets, the sample has a very low birefringence resembling that of an isotropic phase. The different

observation between SAXS and microscopy data may reflect small changes in hydration between the samples. Upon increasing the water content at 50, 70 and 90% (w/w), no sharp scattering peak is observed for β-Mal-C_6C_2 suggesting the system adopts normal micellar solution, L_1 in excess water region. At these concentrations, a two-phase region between water and a liquid-like medium or liquid crystal phase was detected which indicates that an excess water point has been achieved. The SAXS pattern of 90% (w/w) gives a broad peak centered at q of ca. 0.24 $Å^{-1}$, with a lattice parameter or cell−cell distance of 26.7 Å. As shown in Figure 3.7(f), the wide peak indicates absence of long-range crystalline order which can be associated with micellar solution. Due to the short chain length in this compound, the maltose head group plays a dominant effect with its high solubility in water properties resulting in normal micellar solution, L_1 in the excess water region. Comparing the solubility of the maltose-based glycolipid with those of the corresponding glucose counterpart, the solubility of the former is substantially higher (Boyd et al., 2000; Zahid et al., 2013). The surface activity which reflects the strong intramolecular H-bond-driven cohesive forces between sugar headgroup with water will be studied in the future.

For β-Mal-C_8C_4/water system (Figure 3.9(b)), the anisotropic behaviour appeared between 5–67.5% (w/w) at all temperature studied with the excess water point estimated to be around 37.5% (w/w). SAXS data confirm the existence of lamellar phase in this region with the lattice parameter ranging from 32–41 Å. Samples beyond 67.5% (w/w) exhibit fluid isotropic phase between crossed polariser sheets. However, reflection of lamellar phase was observed at 70% (w/w) from SAXS measurement. A single and broad spectrum peaked at q of ca. 0.20$Å^{-1}$ with lattice parameter of 31.1 Å was observed for β-Mal-C_8C_4 at 90% (w/w). This is consistent with the isotropic appearance of the sample. Interestingly, the SAXS scan gave a trace amount of possibly a L_α phase with a d-spacing of 39.8 Å. This could be the results of local drying. The preliminary lyotropic

investigation of β-Mal-C_8C_4 using an optical polarising microscope shows a birefringent texture of L_α phase (see Figure 3.3(d)). Given the fully hydrated sample was equilibrated for at least 14 days, the shorter equilibration times in OPM lyotropic experiment may have disallowed clear visualisation of the L_1 phase since it may take times to form.

As shown in Figure 3.9(c–e), the L_α phase largely dominates the phase behaviour of the middle and longer branched-chain maltosides i.e. β-Mal-$C_{10}C_6$, β-Mal-$C_{12}C_8$ and β-Mal-$C_{14}C_{10}$ in which this phase formation is usually governed by the hydrated headgroup. The excess water point for β-Mal-$C_{10}C_6$ is approximately 40% (w/w), while for β-Mal-$C_{12}C_8$ and β-Mal-$C_{14}C_{10}$, this occurs at slightly lower water content i.e. 37.5% (w/w) and 30% (w/w) respectively. The lattice parameter of the L_α phase ranging from 35–40 Å, 38–43 Å and 42–46 Å respectively. Evidently, an increase in chain length causes an increase in lattice parameter which is accompanied by a shift in the scattering peak position toward lower q values. Such behaviour in lyotropic condition for alkylmaltosides have been reported (Boyd et al., 2000; Milkereit et al., 2005).

Unlike the longer chain Guerbet monosaccharides i.e. β-xylosides and β-glucosides, (with three and four OH groups respectively) which exhibits stable non-lamellar phases such as inverse bicontinuous cubic, V_2 and inverse hexagonal, H_2 in excess water, the corresponding Guerbet disaccharide i.e. β-maltosides (with seven OH groups) favours the formation of L_α phase. This is due to all hydroxyls in maltose are surrounded by extensive water shells (hydration ability), hence, increasing the head group area triggering the formation of the lamellar structure in their fully hydrated systems (Hashim et al., 2012). The results imply that the Guerbet maltosides have the ability to act as membrane forming or membrane stabilising compounds (Ahmad et al., 2012; Ahmad et al., 2014). The lattice parameters for the self-assembly structures in dry and in excess water are summarised in Table 3.4.

Table 3.4: Phase assignments and lattice parameters for the dry and fully hydrated *β*-D-maltosides at 25 °C. Error in lattice parameter measurement is ±0.1 Å. The asterisk, * indicates trace amount.

Lipid	Dry		Fully hydrated	
	Phase	Lattice parameter (Å)	Phase	Lattice parameter (Å)
β-Mal-C_6C_2	L_α	28.1	L_1	26.2
β-Mal-C_8C_4	L_α	29.7	L_1, L_α*	31.4, 39.8*
β-Mal-$C_{10}C_6$	L_α	31.6	L_α	40.2
β-Mal-$C_{12}C_8$	metastable	-	L_α	42.9
β-Mal-$C_{14}C_{10}$	*Ia3d*	89.7	L_α	46.3

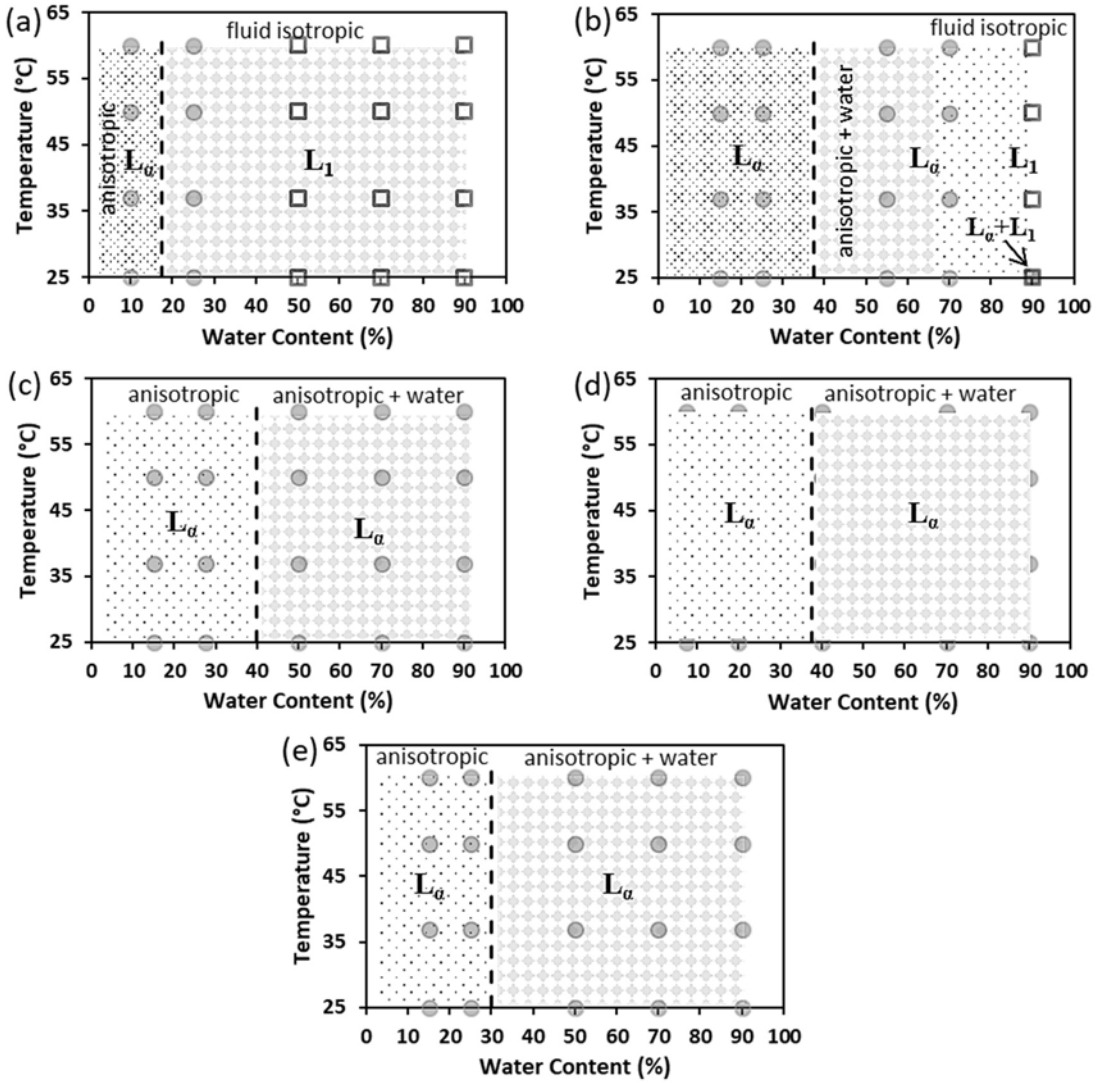

Figure 3.9: Partial binary phase diagrams of *β*-D-maltosides/water on heating: (a) *β*-Mal-C_6C_2; (b) *β*-Mal-C_8C_4; (c) *β*-Mal-$C_{10}C_6$; (d) *β*-Mal-$C_{12}C_8$ and (e) *β*-Mal-$C_{14}C_{10}$. Various phases identified from the SAXS data are marked on the phase diagrams i.e. □ (L_1); ● (L_α) and ■ (L_1 with L_α phase). The coexistence of different phases is also represented by overlapping these notations. Polarising microscopy results are shown in the shaded areas, denoting three distinct shaded regions: anisotropic, fluid isotropic and anisotropic + water. The excess water points are represented by dashed lines.

The temperature dependence of the lattice parameter at selected concentrations for all phases observed in Guerbet *β*-D-maltoside/water phase diagrams is shown in Table 3.5. As mention previously, the lyotropic behaviour was dominated by the L_α phase formation with a few concentrations were found to be in the L_1 phase. The data show that all phases is observed to be invariant with temperature which suggests that there was no significant removal of water molecules from the sugar headgroup as a result of the strong hydrogen bond between the OH groups of the maltoside and water (Stubenrauch, 2001).

Table 3.5: Lattice parameter of *β*-D-maltosides as a function of water content and temperature. Error in lattice parameter measurement is ±0.1 Å.

Compound	Water content (%(w/w))	Lattice parameter (Å)			
		25 °C	37 °C	50 °C	60 °C
β-Mal-C_6C_2	10	28.3	28.4	28.5	28.6
	25	31.1	31.2	31.3	31.3
	50	28.6*	28.6*	28.6*	28.6*
	70	27.3*	27.3*	27.3*	27.3*
	90	26.7*	26.7*	26.7*	26.7*
β-Mal-C_8C_4	15	32.0	32.0	32.0	32.1
	25	34.5	34.4	34.3	34.2
	55	40.0	40.5	40.6	40.6
	70	39.8	40.5	40.6	40.6
	90	40.5, 31.1*	31.1*	31.1*	31.1*
β-Mal-$C_{10}C_6$	15	34.8	34.8	34.8	34.8
	27.5	39.5	39.3	39.1	38.7
	50	40.2	40.2	40.2	40.3
	70	40.0	40.0	40.2	40.2
	90	40.2	40.2	40.3	40.4
β-Mal-$C_{12}C_8$	7.5	38.0	37.9	37.8	37.5
	20	42.9	42.8	42.7	42.7
	40	43.0	43.0	42.8	42.8
	70	42.9	42.8	42.8	42.7
	90	42.9	42.9	42.7	42.6
β-Mal-$C_{14}C_{10}$	15	42.7	42.4	42.1	41.7
	25	46.2	46.0	45.8	45.4
	50	46.3	46.1	45.9	45.9
	70	46.2	46.2	45.9	45.9
	90	46.3	46.1	45.9	45.8

n.b. Asterisk, * indicates lattice parameter for L_1 phase.

CHAPTER 4 : CONCLUSION

In this study, synthesis of high purity β-D-maltosides with chain length -C_6C_2, -C_8C_4, -$C_{10}C_6$, -$C_{12}C_8$ and -$C_{14}C_{10}$ were successfully conducted with verification using NMR spectroscopy. These amphiphilic compounds are amphitropic with large hydrophilic head group that governs most of its liquid crystalline behaviour. The chain length also plays a role in the phase formation as seen in the phase behaviour of longer chain length that gives polymorphism in thermotropic phase study.

The liquid crystalline behaviours were studied using various instrumentation including the DSC, OPM, SAXS and WAXS. In dry condition, the formation of lamellar glass, $L_{\alpha G}$ were observed in the step-shaped T_g transition in DSC thermograms for all compounds. These T_g transitions fall above the room temperature in a rather narrow range of 36 °C and 53 °C. Guerbet maltosides possess higher clearing temperature, T_c than the glucoside counterparts due to the presence of two pyranose sugar rings as its head group which increase the hydrogen bond networks resulting in higher T_c.

The compounds were observed under OPM and the textures of lamellar phase and the subsequent lamellar glass, $L_{\alpha G}$ formed upon cooling were found to be similar before and after T_g. This observation confirms that the molecules were frozen at the T_g and adopt the molecular arrangement before the T_g transitions. Thermotropic polymorphism was observed in the longest chain length due to the equivalently dominant features of the head group and chain branching that result in a more frustrated form of self-assembly. The results from OPM were found to compliment the DSC results within error.

Physicochemical characterisations using SAXS for the first three chain lengths in anhydrous condition reveal the lamellar scattering peak. The fourth chain was found to be kinetically metastable in a wide range of temperature for a long period of time in its dry state. On the other hand, the longest chain i.e. β-Mal-$C_{14}C_{10}$ exhibits polymorphism

over a temperature scan with phase sequence as follows: $L_\alpha \leftrightarrow V_2$ (*Ia*3*d*) $\leftrightarrow H_2$ which was obtained from combined observations of DSC, OPM and SAXS results. In excess water studies, lamellar phase dominates liquid crystalline phase formation of the compounds due to the enlargement of the hydrated head group with the two shorter chains analogue measurement displays the scattering peaks of normal micellar solution. The lamellar phase formation in excess water of these compounds posed a great potential as drug carrier with the formation of multilamellar vesicles.

For future work, focus on these compounds as possible drug carriers and surfactants may be explored as an environmental-friendly base material. Furthermore, further investigation on T_g in lyotropic condition and determination of critical micelle concentration of these compounds will be studied for further understanding of its phase behaviour.

REFERENCES

Ahmad, N., Ramsch, R., Esquena, J., Solans, C., Tajuddin, H. A., & Hashim, R. (2012). Physicochemical characterization of natural-like branched-chain glycosides toward formation of hexosomes and vesicles. *Langmuir, 28*(5), 2395-2403.

Ahmad, N., Ramsch, R., Llinàs, M., Solans, C., Hashim, R., & Tajuddin, H. A. (2014). Influence of nonionic branched-chain alkyl glycosides on a model nano-emulsion for drug delivery systems. *Colloids and Surfaces B: Biointerfaces, 115*, 267-274.

Allen, H. J., & Kisailus, E. C. (1992). *Glycoconjugates: Composition, structure and function*. New York, NY: CRC Press.

Angell, C. A. (1995). Formation of glasses from liquids and biopolymers. *Science, 267*(5206), 1924-1935.

Anthoy, W. (1987). *Solid state chemistry and its applications*. USA: John Wiley & Sons.

Auvray, X., Petipas, C., Dupuy, C., Louvet, S., Anthore, R., Rico-Lattes, I., & Lattes, A. (2001). Small-angle x-ray diffraction study of the thermotropic and lyotropic phases of five alkyl cyclic and acyclic disaccharides: Influence of the linkage between the hydrophilic and hydrophobic moieties. *The European Physical Journal E, 4*(4), 489-504.

Barón, M. (2001). Definitions of basic terms relating to low-molar-mass and polymer liquid crystals (IUPAC Recommendations 2001). *Pure and Applied Chemistry, 73*(5), 845-895.

Bayach, I., Manickam Achari, V., Wan Iskandar, W. F. N., Sugimura, A., & Hashim, R. (2016). Computational insights into octyl-D-xyloside isomers towards understanding the liquid crystalline structure: Physico-chemical features. *Liquid Crystals, 43*(10), 1503-1513.

Bonicelli, M., Ceccaroni, G., & La Mesa, C. (1998). Lyotropic and thermotropic behavior of alkylglucosides and related compounds. *Colloid and Polymer Science, 276*(2), 109-116.

Borsali, R., & Pecora, R. (2008). *Soft-matter characterization*. New York, NY: Springer Science+Business Media.

Boyd, B. J., Drummond, C. J., Krodkiewska, I., & Grieser, F. (2000). How chain length, headgroup polymerization, and anomeric configuration govern the thermotropic and lyotropic liquid crystalline phase behavior and the air-water interfacial adsorption of glucose-based surfactants. *Langmuir, 16*(19), 7359-7367.

Brooks, N. J., Hamid, H. A., Hashim, R., Heidelberg, T., Seddon, J. M., Conn, C. E., Mirzadeh Husseini, S. M., Zahid, N. I., & Hussen, R. S. D. (2011). Thermotropic and lyotropic liquid crystalline phases of Guerbet branched-chain-D-glucosides. *Liquid Crystals, 38*(11-12), 1725-1734.

Brown, G., & Wolken, J. (1979). *Liquid crystals and biological structures*. New York, NY: Academic Press.

Carlton, R. A. (2011). *Pharmaceutical microscopy*. New York, NY: Springer Science+Business Media.

Castellano, J. A. (2005). *Liquid gold: The story of liquid crystal displays and the creation of an industry*. Singapore: World Scientific.

Chen, S., Katsis, D., Schmid, A., Mastrangelo, J., Tsutsui, T., & Blanton, T. (1999). Circularly polarized light generated by photoexcitation of luminophores in glassy liquid-crystal films. *Nature, 397*(6719), 506.

Chester, M. A. (1999). IUPAC-IUB joint commission on biochemical nomenclature (JCBN) nomenclature of glycolipids: Recommendations 1997. *Journal of Molecular Biology, 286*(3), 963-970.

Collings, P. J. (2002). *Liquid crystals: Nature's delicate phase of matter*. United Kingdom: Princeton University Press.

Collings, P. J., & Hird, M. (1997). *Introduction to liquid crystals: Chemistry and physics*. London, England: Taylor & Francis.

Curatolo, W. (1987). The physical properties of glycolipids. *Biochimica et Biophysica Acta (BBA)-Reviews on Biomembranes, 906*(2), 111-136.

de Gennes, P., & Prost, I. (1993). *The physics of liquid crystals* (2nd ed.). New York, NY: Oxford University Press.

Dierking, I. (2003). *Textures of liquid crystals*. Federal Republic of Germany: John Wiley & Sons.

Dziedzic, S., & Kearsley, M. (1984). *Glucose syrups: Science and technology*. London, England: Elsevier Applied Science Publishers.

Ellens, H., Bentz, J., & Szoka, F. C. (1986). Fusion of phosphatidylethanolamine-containing liposomes and mechanism of the L_{α}–H_{II} phase transition. *Biochemistry, 25*(14), 4141-4147.

Elliott, S. R. (1990). *Physics of amorphous materials*. United Kingdom: Longman Scientific & Technical.

Ericsson, C. A., Ericsson, L. C., Kocherbitov, V., Söderman, O., & Ulvenlund, S. (2005). Thermotropic phase behaviour of long-chain alkylmaltosides. *Physical Chemistry Chemical Physics, 7*(15), 2970-2977.

Ericsson, C. A., Ericsson, L. C., & Ulvenlund, S. (2005). Solid-state phase behaviour of dodecylglycosides. *Carbohydrate Research, 340*(8), 1529-1537.

Ezquerra, T. A., Garcia-Gutierrez, M. C., Nogales, A., & Gomez, M. (2009). *Applications of synchrotron light to scattering and diffraction in materials and life sciences* (Vol. 776). Berlin, Heidelberg: Springer.

Friedel, G. (1922). Les états mésomorphes de la matière. *Ann. Phys., 9*(18), 273-474.

Fukumasa, M., Kato, T., Uryu, T., & Fréchet, J. M. (1993). The simplest structure of the hydrogen-bonded mesogen built from 4-alkoxybenzoic acid and 4-alkylpyridine. *Chemistry Letters, 22*(1), 65-68.

Gabbott, P. (2008). *Principles and applications of thermal analysis*. Oxford, United Kingdom: Blackwell Publishing Ltd.

Garden, J.-L., & Bourgeois, O. (2012). Nanocalorimetry. In B. Bhushan (Ed.), *Encyclopedia of nanotechnology* (pp. 1491-1504). Dordrecht: Springer Netherlands.

Garidel, P., Howe, J., Milkereit, G., Rössle, M., Linser, S., Gerber, S., Willumeit, R., Gutsmann, T., Vill, V., & Brandenburg, K. (2008). Structural polymorphism of hydrated ether-linked dimyristyl maltoside and melibioside. *Chemistry and Physics of Lipids, 151*(1), 18-29.

Garidel, P., Kaconis, Y., Heinbockel, L., Wulf, M., Gerber, S., Munk, A., Vill, V., & Brandenburg, K. (2015). Self-organisation, thermotropic and lyotropic properties of glycolipids related to their biological implications. *The Open Biochemistry Journal, 9*, 49.

Goodby, J. W. (1998). Liquid crystals and life. *Liquid Crystals, 24*(1), 25-38.

Goodby, J. W. (2012). Introduction to defect textures in liquid crystals. In J. Chen, W. Cranton & M. Fihn (Eds.), *Handbook of visual display technology* (pp. 1289-1314). Berlin, Heidelberg: Springer Berlin Heidelberg.

Gray, G. W. (1962). *Molecular structure and the properties of liquid crystals*. London, England: Academic press.

Hamley, I. (2000). *Introduction to soft matter: Polymers, colloids, amphiphiles and liquid crystals*. England: John Wiley & Sons.

Hashim, R., Hashim, H. H. A., Rodzi, N. Z. M., Hussen, R. S. D., & Heidelberg, T. (2006). Branched chain glycosides: Enhanced diversity for phase behavior of easily accessible synthetic glycolipids. *Thin Solid Films, 509*(1), 27-35.

Hashim, R., Sugimura, A., Minamikawa, H., & Heidelberg, T. (2012). Nature-like synthetic alkyl branched-chain glycolipids: A review on chemical structure and self-assembly properties. *Liquid Crystals, 39*(1), 1-17.

Hashim, R., Zahid, N. I., Velayutham, T. S., Aripin, N. F. K., Ogawa, S., & Sugimura, A. (2018). Dry thermotropic glycolipid self-assembly: A review. *Journal of Oleo Science, 67*(6), 651-668.

Hassan, H. (2001). *Synthesis and liquid crystal phase behaviour of branched chain alkyl glycosides.* (PhD's Thesis), Universtiy of Malaya.

Hato, M., Yamashita, J., & Shiono, M. (2009). Aqueous phase behavior of lipids with isoprenoid type hydrophobic chains. *The Journal of Physical Chemistry B, 113*(30), 10196-10209.

Helfrich, W., & Heppke, G. (1980). *Liquid crystals of one-and two-dimensional order: Proceedings of the conference on liquid crystals of one-and two-dimensional order and their applications, Garmisch-Partenkirchen, Federal Republic of Germany, January 21–25, 1980* (Vol. 11). Berlin: Springer-Verlag.

Imamura, K., Ogawa, T., Sakiyama, T., & Nakanishi, K. (2003). Effects of types of sugar on the stabilization of protein in the dried state. *Journal of Pharmaceutical Sciences, 92*(2), 266-274.

Israelachvili, J. N. (2015). *Intermolecular and surface forces* (3rd ed.). USA: Academic Press.

Jeffrey, G. A. (1986). Carbohydrate liquid crystals. *Accounts of Chemical Research, 19*(6), 168-173.

Kaasgaard, T., & Drummond, C. J. (2006). Ordered 2-D and 3-D nanostructured amphiphile self-assembly materials stable in excess solvent. *Physical Chemistry Chemical Physics, 8*(43), 4957-4975.

Kauzmann, W. (1948). The nature of the glassy state and the behavior of liquids at low temperatures. *Chemical Reviews, 43*(2), 219-256.

Kelly, A., & Knowles, K. M. (2012). Amorphous materials and special types of crystal–solid aggregates. In *Crystallography and crystal defects* (pp. 123-140): John Wiley & Sons, Ltd.

Kitamoto, D., Morita, T., Fukuoka, T., Konishi, M.-a., & Imura, T. (2009). Self-assembling properties of glycolipid biosurfactants and their potential applications. *Current Opinion in Colloid & Interface Science, 14*(5), 315-328.

Kocherbitov, V., & Söderman, O. (2004). Glassy crystalline state and water sorption of alkyl maltosides. *Langmuir, 20*(8), 3056-3061.

Kocks, U. F., Tomé, C. N., Wenk, H.-R., & Beaudoin, A. J. (1998). *Texture and anisotropy: Preferred orientations in polycrystals and their effect on materials properties*. United Kingdom: Cambridge University Press.

Kulkarni, C. V., Wachter, W., Iglesias-Salto, G., Engelskirchen, S., & Ahualli, S. (2011). Monoolein: A magic lipid? *Physical Chemistry Chemical Physics, 13*(8), 3004-3021.

Kumar, S. (2011). *Chemistry of discotic liquid crystals: From monomers to polymers*. USA: CRC press.

Laver, M. (2012). Small-angle scattering of nanostructures and nanomaterials. In B. Bhushan (Ed.), *Encyclopedia of nanotechnology* (pp. 2437-2450). Dordrecht: Springer Netherlands.

Lehmann, O. (1889). Über fliessende krystalle. *Zeitschrift für Physikalische Chemie, 4*(1), 462-472.

Liao, G., Zewe, S., Hagerty, J., Hashim, R., Abeygunaratne, S., Vill, V., & Jákli, A. (2006). Thermotropic liquid crystalline properties of amphiphilic branched chain glycolipids. *Liquid Crystals, 33*(3), 361-366.

Liew, C. Y. (2016). *Synthesis and characterisation of biomass derived Guerbet branched-chain xylose glycolipids.* (Master Dissertation), University of Malaya.

Liew, C. Y., Salim, M., Zahid, N. I., & Hashim, R. (2015). Biomass derived xylose Guerbet surfactants: Thermotropic and lyotropic properties from small-angle X-ray scattering. *RSC Advances, 5*(120), 99125-99132.

Lindhorst, T. K. (2000). *Essentials of carbohydrate chemistry and biochemistry*. New York, NY: Wiley-Vch New York.

Manickam Achari, V., Nguan, H. S., Heidelberg, T., Bryce, R. A., & Hashim, R. (2012). Molecular dynamics study of anhydrous lamellar structures of synthetic glycolipids: Effects of chain branching and disaccharide headgroup. *The Journal of Physical Chemistry B, 116*(38), 11626-11634.

ManickamAchari, V., Bryce, R. A., & Hashim, R. (2014). Conformational dynamics of dry lamellar crystals of sugar based lipids: An atomistic simulation study. *Plos One, 9*(6), e101110.

Mannock, D., & McElhaney, R. (2004). Thermotropic and lyotropic phase properties of glycolipid diastereomers: Role of headgroup and interfacial interactions in determining phase behaviour. *Current Opinion in Colloid & Interface Science, 8*(6), 426-447.

Mannock, D. A., Collins, M. D., Kreichbaum, M., Harper, P. E., Gruner, S. M., & McElhaney, R. N. (2007). The thermotropic phase behaviour and phase structure of a homologous series of racemic *β*-D-galactosyl dialkylglycerols studied by differential scanning calorimetry and X-ray diffraction. *Chemistry and Physics of Lipids, 148*(1), 26-50.

marketsandmarkets.com. (October 2016). Surfactants Market by Type (Anionic, Non-Ionic, Cationic, and Amphoteric), Substrate (Synthetic, and Bio-based), Application (Detergents, Personal Care, Textile, Elastomers & Plastics, Crop Protection, Food & Beverage) - Global Forecast to 2021. CH 3464. Retrieved 5 February, 2018, from https://www.marketsandmarkets.com/Market-Reports/biosurfactants-market-493.html

Menczel, J. D., & Prime, R. B. (2009). *Thermal analysis of polymers: Fundamentals and applications*. New Jersey: John Wiley & Sons.

Milkereit, G., Brandenburg, K., Gerber, S., Koch, M., Morr, M., Andra, J., Seydel, U., & Vill, V. (2005). Synthesis and mesomorphic properties of glycosyl dialkyl-and diacyl-glycerols bearing saturated, unsaturated and methyl branched fatty acid and fatty alcohol chains: Part II: Mesomorphic properties. *Chemistry and Physics of Lipids, 135*(1), 15-36.

Minamikawa, H., & Hato, M. (1998). Reverse micellar cubic phase in a phytanyl-chained glucolipid/water system. *Langmuir, 14*(16), 4503-4509.

Nagarajan, R. (2002). Molecular packing parameter and surfactant self-assembly: The neglected role of the surfactant tail. *Langmuir, 18*(1), 31-38.

Nainggolan, I., Radiman, S., Hamzah, A. S., & Hashim, R. (2009). The effect of the head group on branched-alkyl chain surfactants in glycolipid/n-octane/water ternary system. *Colloids and Surfaces B: Biointerfaces, 73*(1), 84-91.

Nilsson, F., Söderman, O., & Johansson, I. (1997). Physical-chemical properties of some branched alkyl glucosides. *Langmuir, 13*(13), 3349-3354.

Noel, T. R., Parker, R., & Ring, S. G. (2000). Effect of molecular structure and water content on the dielectric relaxation behaviour of amorphous low molecular weight carbohydrates above and below their glass transition. *Carbohydrate Research, 329*(4), 839-845.

Noh, J., Reguengo De Sousa, K., & Lagerwall, J. P. F. (2016). Influence of interface stabilisers and surrounding aqueous phases on nematic liquid crystal shells. *Soft Matter, 12*(2), 367-372.

Norde, W. (2011). *Colloids and interfaces in life sciences and bionanotechnology*. USA: CRC Press.

Ogawa, S., Asakura, K., & Osanai, S. (2013). Thermotropic and glass transition behaviors of n-alkyl *β*-D-glucosides. *RSC Advances, 3*(44), 21439-21446.

Ogawa, S., & Osanai, S. (2012). Glass transition behavior of aqueous solution of sugar-based surfactants. In P. Wilson (Ed.), Supercooling: IntechOpen.

Pabst, G., Heberle, F. A., & Katsaras, J. (2013). X-ray scattering of lipid membranes. In G. C. K. Roberts (Ed.), *Encyclopedia of biophysics* (pp. 2785-2791). Berlin, Heidelberg: Springer Berlin Heidelberg.

Patrick, M., Zahid, N. I., Kriechbaum, M., & Hashim, R. (2018). Guerbet glycolipids from mannose: Liquid crystals properties. *Liquid Crystals*, 1-17.

Pecharsky, V. K., & Zavalij, P. Y. (2009). *Fundamentals of powder diffraction and structural characterization of materials* (Vol. 69). New York, NY: Springer.

Reinitzer, F. (1989). Contributions to the knowledge of cholesterol. *Liquid Crystals, 5*(1), 7-18.

Robinson, P. C., Davidson, M. W. (2016). Polarized Light Microscopy. Retrieved 10 November, 2016, from https://www.microscopyu.com/techniques/polarized-light/polarized-light-microscopy

Sagnella, S. M., Conn, C. E., Krodkiewska, I., Mulet, X., & Drummond, C. J. (2011). Anandamide and analogous endocannabinoids: A lipid self-assembly study. *Soft Matter, 7*(11), 5319-5328.

Salim, M., Wan Iskandar, W. F. N., Patrick, M., Zahid, N. I., & Hashim, R. (2016). Swelling of bicontinuous cubic phases in Guerbet glycolipid: Effects of additives. *Langmuir*.

Saupe, A. (1977). Textures, deformations, and structural order of liquid crystals. *Journal of Colloid and Interface Science, 58*(3), 549-558.

Seddon, J. M. (1990). Structure of the inverted hexagonal (H_{II}) phase, and non-lamellar phase transitions of lipids. *Biochimica et Biophysica Acta (BBA) - Reviews on Biomembranes, 1031*(1), 1-69.

Shearman, G. C., Ces, O., Templer, R. H., & Seddon, J. M. (2006). Inverse lyotropic phases of lipids and membrane curvature. *Journal of Physics: Condensed Matter, 18*(28), S1105.

Singh, S., & Dunmur, D. A. (2002). *Liquid crystals: Fundamentals*. Singapore: World Scientific.

Stubenrauch, C. (2001). Sugar surfactants — aggregation, interfacial, and adsorption phenomena. *Current Opinion in Colloid & Interface Science, 6*(2), 160-170.

Suga, H. (2011). Introduction: Some essential attributes of glassiness regarding the nature of non-crystalline solids. In J. Šesták, J. J. Mareš & P. Hubík (Eds.), *Glassy, amorphous and nano-crystalline materials: thermal physics, analysis, structure and properties* (pp. 1-19). Dordrecht: Springer Netherlands.

Tenchov, B. (1991). On the reversibility of the phase transitions in lipid-water systems. *Chemistry and Physics of Lipids, 57*(2-3), 165-177.

Tschierske, C. (2002). Liquid crystalline materials with complex mesophase morphologies. *Current Opinion in Colloid & Interface Science, 7*(1), 69-80.

Tyler, A. I. I., Law, R. V., & Seddon, J. M. (2015). X-Ray diffraction of lipid model membranes. In M. D. Owen (Ed.), *Methods in membrane lipids* (pp. 199-225). New York, NY: Springer New York.

Vill, V., Böcker, T., Thiem, J., & Fischer, F. (1989). Studies on liquid-crystalline glycosides. *Liquid Crystals, 6*(3), 349-356.

Vill, V., & Hashim, R. (2002). Carbohydrate liquid crystals: Structure–property relationship of thermotropic and lyotropic glycolipids. *Current Opinion in Colloid & Interface Science, 7*(5), 395-409.

Vill, V., von Minden, H., Koch, M., Seydel, U., & Brandenburg, K. (2000). Thermotropic and lyotropic properties of long chain alkyl glycopyranosides. Part I: Monosaccharide headgroups. *Chemistry and Physics of Lipids, 104*(1), 75-91.

von Minden, H., Brandenburg, K., Seydel, U., Koch, M., Garamus, V., Willumeit, R., & Vill, V. (2000). Thermotropic and lyotropic properties of long chain alkyl glycopyranosides. Part II: Disaccharide headgroups. *Chemistry and Physics of Lipids, 106*(2), 157-179.

Wiesenauer, B. R., & Gin, D. L. (2012). Nanoporous polymer materials based on self-organized, bicontinuous cubic lyotropic liquid crystal assemblies and their applications. *Polymer Journal, 44*(6), 461.

Williams, D. B., & Carter, C. B. (2009). *Transmission electron microscopy: A textbook for materials science*. New York, NY: Springer Science+Business Media.

Wojtowicz, P. J., Sheng, P., & Priestley, E. (1975). *Introduction to liquid crystals*. London, England: Plenum Press.

Wood, E. A. (1977). *Crystals and light: An introduction to optical crystallography*. New York, NY: Dover Publication, Inc.

Zahid, N. I., Conn, C. E., Brooks, N. J., Ahmad, N., Seddon, J. M., & Hashim, R. (2013). Investigation of the effect of sugar stereochemistry on biologically relevant lyotropic phases from branched-chain synthetic glycolipids by small-angle x-ray scattering. *Langmuir, 29*(51), 15794-15804.

Zahid, N. I. (2013). *Investigation of glycolipids self-assemblies using fluorescence spectroscopy and small-angle x-ray scattering.* (PhD's Thesis), University of Malaya.

Zhang, Z., Fukunaga, K., Sugimura, Y., Nakao, K., & Shimizu, T. (1996). Synthesis of glycolipids: dialkyl N-[N-(4-lactonamidobutyl) succinamoyl] l-glutamates. *Carbohydrate Research, 290*(2), 225-232.

LIST OF PUBLICATIONS AND PAPERS PRESENTED

Publication

Academic Journal

Saari, N. A. N., Mislan, A. A., Hashim, R., & Zahid, N. I. (2018). Self-assembly, thermotropic, and lyotropic phase behavior of Guerbet branched-chain maltosides. *Langmuir, 34*(30), 8962-8974.

Zahid, N. I., Abou-Zied, O. K., Saari, N. A. N., & Hashim, R. (2016). Comparative study of the inverse versus normal bicontinuous cubic phases of the *β*-D-glucopyranoside water-driven self-assemblies using fluorescent probes. *RSC Advances, 6*(1), 227-235.

Presentation

Poster

Liquid Crystalline Properties of Synthetic Branched-chain Glycolipids, 7th Asian Conference on Colloid and Interface Science (ACCIS 2017), 8–11th August 2017, Kuala Lumpur, Malaysia (Best Poster Presentation Award).